Investigation of Fusion Reactions of Heavy Ions And Development of Necessary Instrumentation

A Thesis submitted to the University of Calicut
for the partial fulfillment of the requirements
for the degree of
Doctor of Philosophy in Physics

Ajith Kumar B.P.

Department of Physics
University of Calicut
May, 2007

Investigation of Fusion Reactions of Heavy Ions And Development of Necessary Instrumentation

A Thesis submitted to the University of Calicut
for the partial fulfillment of the requirements
for the degree of
Doctor of Philosophy in Physics

Ajith Kumar B.P.

Department of Physics
University of Calicut
May, 2007

CERTIFICATE

This is to certify that this thesis entitled "Investigation of Fusion Reactions of Heavy Ions and Development of Necessary Instrumentation" is a bona-fide record of research work carried out by Ajith Kumar B.P. under my supervision in the Department of Physics, University of Calicut, for the award of the Ph. D degree of University of Calicut and that no part of this thesis has been presented elsewhere for the award of any degree, diploma or other similar title.

K. M. Varier

Calicut University
5th May 2007

(Dr. K. M. Varier)

Investigation of Fusion Reactions of Heavy Ions And Development of Necessary Instrumentation

A Thesis submitted to the University of Calicut
for the partial fulfillment of the requirements
for the degree of
Doctor of Philosophy in Physics

Ajith Kumar B.P.

Department of Physics
University of Calicut
May, 2007

DECLARATION

I hereby declare that this thesis entitled "Investigation of Fusion Reactions of Heavy Ions and Development of Necessary Instrumentation" is a bona-fide record of research work done by me and that no part of this thesis has been presented before for the award of any degree or diploma.

Ajith

Calicut University
5th May 2007

(Ajith Kumar B.P.)

Investigation of Fusion Reactions of Heavy Ions And Development of Necessary Instrumentation

A Thesis submitted to the University of Calicut
for the partial fulfillment of the requirements
for the degree of
Doctor of Philosophy in Physics

Ajith Kumar B.P.

Department of Physics
University of Calicut
May, 2007

Dedicated

to the

Education System

which I am indebted to

Investigation of Fusion Reactions of Heavy Ions And Development of Necessary Instrumentation

A Thesis submitted to the University of Calicut
for the partial fulfillment of the requirements
for the degree of
Doctor of Philosophy in Physics

Ajith Kumar B.P.

Department of Physics
University of Calicut
May, 2007

Acknowledgments

I express my sincere thanks to my thesis supervisor Dr. K.M.Varier who helped me gain some understanding about the field and also took the trouble of traveling to Delhi and Mumbai to participate in the lengthy experiments. Without the support of Dr. S. Kailas it would not have been possible for me to complete this work. I thank him for the encouragement and guidance he provided throughout this work.

Discussions with Dr.S.K.Dutta helped me a lot to get some idea about the subject. I also thank him for the help provided during the initial experiments done at IUAC, Delhi. I thank Dr.A.K.Sinha for his support for the experiments carried out during this work. I thank Prof.G.K.Mehta for the help provided to get this work started and for the constant reminders to finish it in time.

Help from my colleagues at IUAC and BARC, has been crucial in completing this work and also learning about experimental techniques. I am grateful to Sugathan, Madhavan, Akhil, Muralithar, Subir Nath, Pradeep Barua and Jimson for the support and help they provided during the experiments.

I am grateful to Bency John and Renji Thomas for the time spent with them, which was rewarding in many ways. I thank Alok Saxena, Kripa Mahata, D.C.Biswas and B.K.Nayak for participating in the experiments and all other help they provided.

I thank Antony Joseph for keeping my registration alive, the 'local guardian' always paid the fee in time. A.M.Vinod Kumar has been very helpful in many aspects including looking for bugs in 'Freedom' . Thanks to Ison, Madhusudhana Rao and Pramode for various helps.

The cooperation and support from the operations staff at TIFR and IUAC Pelletrons are highly acknowledged. There are many others, including my family, who provided direct and indirect help during this work and I thank them all.

Ajith Kumar

Investigation of Fusion Reactions of Heavy Ions
And
Development of Necessary Instrumentation

A Thesis submitted to the University of Calicut
for the partial fulfillment of the requirements
for the degree of
Doctor of Philosophy in Physics

Ajith Kumar B.P.

Department of Physics
University of Calicut
May, 2007

Contents

Investigation of Fusion Reactions of Heavy Ions And Development of Necessary Instrumentation

A Thesis submitted to the University of Calicut
for the partial fulfillment of the requirements
for the degree of
Doctor of Philosophy in Physics

Ajith Kumar B.P.

Department of Physics
University of Calicut
May, 2007

List of Figures

Investigation of Fusion Reactions of Heavy Ions And Development of Necessary Instrumentation

A Thesis submitted to the University of Calicut
for the partial fulfillment of the requirements
for the degree of
Doctor of Philosophy in Physics

Ajith Kumar B.P.

Department of Physics
University of Calicut
May, 2007

List of Tables

Investigation of Fusion Reactions of Heavy Ions And Development of Necessary Instrumentation

A Thesis submitted to the University of Calicut
for the partial fulfillment of the requirements
for the degree of
Doctor of Philosophy in Physics

Ajith Kumar B.P.

Department of Physics
University of Calicut
May, 2007

List of Publications/Presentations

1. Fission fragment angular distribution of ^{13}C+^{232}Th system at near barrier energies.
   B.P. Ajith Kumar, K.M.Varier, R.G.Thomas,K.mahata,B.V.John, A.Saxena,Rajprakash and S.Kailas.
   Phy. Rev. C. Vol 72(2005)

2. Fission fragment angular distribution of ^{13}C+^{232}Th system at near Coulomb barrier energies.
   B.P. Ajith Kumar, K.M.Varier, Bency John, A.Saxena, D.C.Biswas, B.K.Nayak and S.Kailas.
   Proc. of the DAE/BRNS Symp. on Nucl. phy. (2006)

3. Fission fragment angular distribution of ^{13}C+^{232}Th,235U systems around the fusion barrier
   K.M.Varier, *B.P. Ajith Kumar*, K.Mahata, B.V. John, A.Saxena, S.Kailas and Rajprakash.
   Proc. of the DAE/BRNS Symp. on Nucl. phy. (2003)

4. Fission fragment anisotropies in the of ^{12,13}C+^{232}Th system at near and sub barrier energies.
   B.P. Ajith Kumar, K.M.Varier, A.K.Sinha, S.K.Dutta, N.Madhavan, P.Sugathan, Subir Nath, P.Barua, P.V.Madhusudhana rao, S.Kailas, B.Krishnarajalu & Raghubir Singh.
   Proc. of the DAE/BRNS Symp. on Nucl. phy. (2001)

5. One and two proton transfer reaction in the ^{12,13}C+^{232}Th systems at near and sub barrier energies
   K.V.Chacko, K.P.Chandrasekharan, Charlie Kattakkayam, K.M.Varier, *B.P.Ajith Kumar*, A.K.Sinha, S.K.Dutta, N.Madhavan, P.Sugathan, A.Jinghan, Subir Nath, P.Barua, P.V.Madhusudhana rao, S.Kailas, B.Krishnarajalu & Raghubir Singh.
   Proc. of the DAE/BRNS Symp. on Nucl. phy. (2001)

6. Elastic and inelastic scattering in the $^{12,13}C+^{235}U$ system at near and sub barrier energies.
   K.P.Chandrasekharan, K.V.Chacko, Charlie Kattakkayam, K.M.Varier, *B.P.Ajith Kumar*, A.K.Sinha, S.K.Dutta, N.Madhavan, P.Sugathan, A.Jinghan, Subir Nath, P.Barua, P.V.Madhusudhana rao, S.Kailas, B.Krishnarajalu & Raghubir Singh. Proc. of the DAE/BRNS Symp. on Nucl. phy. (2001)

7. A high speed distributed data Acquisition System.
   B.P. Ajith Kumar, E.T.Subrahmaniam, Kusum Rani and Kundan Singh. Proc. of the DAE/BRNS Symp. on Nucl. phy. (2001)

8. A Linux based data acquisistion system at NSC.
   B.P.Ajith Kumar, E.T.Subrahmaniam & Sumit Mookerji,
   Proc. of Symp. on Advances in Nuclear and Allied Instrumentation, BARC, Feb(1997)

Investigation of Fusion Reactions of Heavy Ions And Development of Necessary Instrumentation

A Thesis submitted to the University of Calicut
for the partial fulfillment of the requirements
for the degree of
Doctor of Philosophy in Physics

Ajith Kumar B.P.

Department of Physics
University of Calicut
May, 2007

Chapter 1

Introduction

In nuclear physics, the process of more than one nuclei joining together to form a heavier nucleus is called fusion, energy is absorbed or released depending on the masses of the nulcei involved. Fusion resulting in a nucleus of mass up to iron releases energy and above that energy is absorbed. However, in both cases a good amount of energy is required to overcome the mutual Coulomb repulsion between the incoming nuclei before bringing them within the range of attractive nuclear forces so that they can fuse together. The nuclei must approach each other with enough kinetic energy to overcome the Coulomb repulsion. At high temperatures, like that of a star, the average kinetic energy is sufficient to overcome the Coulomb barrier whereas in laboratory experiments a particle accelerator is required to generate high energy projectiles. Due to the initial kinetic energy and the binding energy released the nuclei produced will be mostly in some excited state and will decay through various processes. What we experimentally observe is the final reaction products but the formation of an intermediate system is assumed. Niels Bohr introduced the concept of a compound nucleus [Bohr 1936] to explain certain class of nuclear reactions. The target and projectile is assumed to fuse together to form a composite system, that is not stable in the macroscopic time scale but lasts for a time that is long compared to the nuclear transit-time. The compound nucleus decays by emitting γ-rays, light particles or by fission. The kinetic energy of the projectile is converted into

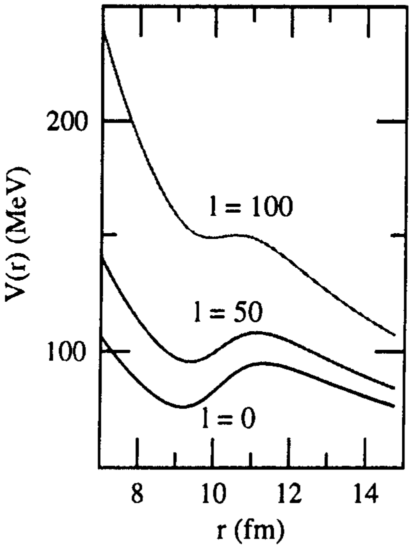

Figure 1.1: One dimensional potential for several ℓ values calculated. Coulomb potential is calculated assuming point mass and the nuclear part from Wood-Saxon potential.

the excitation energy and angular momentum of the compound nucleus.

A simple theoretical explanation for fusion can be given in terms of a one dimensional potential barrier formed by the repulsive Coulomb and centrifugal potentials and the attractive nuclear potential as shown in figure 1.1. The compound nucleus is formed by trapping the ions in the potential energy pocket. The angular momentum of the composite system is decided by the impact parameter. For higher angular momentum values the pocket becomes shallower and finally vanishes, setting an upper limit for the angular momentum of the compound nucleus. For very heavy nuclei, having Z^2/A values greater than 45, the composite system breaks up immediately without forming a compound nucleus. For projectile energies slightly below the barrier also fusion takes place, due to the quantum tunneling through the barrier. The height, shape and position of the barrier are described in terms of few parameters obtained by fitting the fusion cross section data. Various types of potentials have been used to explain the experimental data with varying degrees of success.[Krappe 1979, Vaz 1978]

It has been observed that the experimental results do not exactly conform to the one dimensional barrier model [Beckerman 1988, Dasgupta 1998], especially at below barrier energies. This implies that viewing the fusion process as two structureless spheres interacting through the inter-nuclear potential is inadequate. The coupling of the internal degrees of freedom with the translational motion also need to be considered. The effect of such coupling can be easily visualized by attributing their effect to the replacement of the single barrier with a distribution of barriers having different heights. It is possible to extract this distribution of barriers from the measured fusion excitation function $\sigma(E)$, by taking the second derivative of $E\sigma(E)$ with respect to E. This method has been used extensively to extract the barrier distribution from experimental data and interpret it in terms of the coupling with various internal degrees of freedom like vibration, rotation etc. [Dasso 1983]

In the study of fusion reactions the experimental observables are the fusion cross section $\sigma(E)$ and the moments of angular momenta $\ell(E)$, providing valuable information about reaction dynamics and nuclear structure. The total fusion cross section is obtained by measuring the cross sections for possible modes of decay: evaporation and fission. For light systems evaporation is the dominant decay mode whereas for heavy systems fission predominates. For intermediate masses these two processes compete each other. Angular momentum distributions are deduced from gamma ray multiplicities or by measuring the relative population of the ground and isomeric states of the compound nucleus.

In this study we are investigating actinide nuclei whose main mode of decay is by fission. The fission process was explained by Bohr [Bohr 1939] based on the liquid drop nuclear model. The compound nucleus formed by the fusion process undergoes shape oscillations due to the available excitation energy. The repulsive Coulomb force tends to increase the deformation from spherical shape while the nuclear surface force tries to reduce the deformation, in-order to minimize the surface area. The deformation at which these to forces balance each other is called the saddle point shape. Once the deformation exceeds this level the nucleus undergoes fission. Probability of fission also depends on the Z^2/A value and the available excitation energy. Massive systems can undergo fission even with zero excitation energy due to quantum tunneling as evident from the spontaneous fission phenomena.

An important experimental observable in the study of induced fission is the angular distribution of the fission fragments. It was postulated by A.Bohr [A Bohr 1956] that the kinetic energy brought in by the projectile goes mostly in to the deformation degrees of freedom of the compound nucleus. Since only small amount of the available energy is spent on the excitation, at low projectile energies the energy levels of the compound nucleus are comparable to that of a ground state nucleus. This implies that at excitation energies comparable to the fission barrier, the fission occurs only through few channels. Bohr formulated a simple relationship between the angular momentum J of the compound nucleus, its projection K along the nuclear symmetry axis and the angular distribution of fission fragments. It is assumed that the fission fragments separate along the symmetry axis of the saddle point nucleus and the K distribution is unchanged from saddle to scission. Parameters describing the shape of compound nucleus at saddle point can be extracted from the fission fragment angular distribution data.

Bohr's hypothesis was extended by Halpern and Strutinsky [Halpern 1957] to higher excitation energies, where the transition levels can be described by statistical methods, leading to the Statistical Saddle Point Model (SSPM) [Vandenbosch] . The fragment angular distribution can be obtained by summing over all possible values of J and K with proper weighting using the density of levels calculated using statistical methods. According to SSPM theory the anisotropy of fragment angular distribution is related to the second moment of the spin distribution and the variance K_0^2 of the projection of the total angular momentum along the nuclear symmetry axis. The value of K_0^2 in turn depends on the effective moment of inertia, a function of deformation, and the temperature of the saddle point nucleus. SSPM theory assumes that a fully equilibrated compound nucleus is formed before fissioning takes place. The measured anisotropies of fragment angular distribution by using light projectiles were explained satisfactorily by SSPM.

However, the results of experiments carried out using heavy projectiles, which became available with the advent of heavy ion accelerators in the eighties, showed deviations from the SSPM predictions. This triggered a new interest in the study of fragment angular distribution which is expected to throw some light in to the dynamics of the fusion-fission process. Several theories have been put forward to explain the deviations from SSPM, proposing different modes of fission that takes place without the formation of a fully equilibrated compound nucleus. Non-Compound Nucleus Fission (NCNF) mechanisms like fast fission (FF), quasi-fission (QF) [Back 1985] and pre-equilibrium fission (PEF) [Ramamurthy 1985] has been proposed by various groups. Large amount of experimental data has been gathered over the years to investigate the effects of target and projectile spins, ratio of their masses, etc. on the nature of compound nucleus formation and the modes of decay [Kailas 1997].

When a heavy target and light projectile nuclei come in contact, they proceed towards the formation of a compound nucleus provided that the initial mass flow is from the projectile to the target. As we increase the projectile mass at some point the direction of mass flow changes and fission occurs through the formation of a di-nucleus. The value of mass asymmetry $\alpha = (A_T - A_P)/(A_T + A_P)$ where the mass flow changes direction is called the Businaro-Gallone critical mass asymmetry α_{BG} [Businaro 1955]. For values of $\alpha < \alpha_{BG}$, the contribution of Non-Compound Nucleus fission events becomes significant and the anisotropies deviate from the SSPM values.

Another interesting observation was the increased anisotropy observed at near-barrier energies for deformed actinide targets. This was explained by the orientation dependent quasi-fission model [Hinde 1996] according to which the probability of compound nucleus formation depends on the angle between the beam direction and the symmetry axis of the target nucleus, ie. collisions with the tip of the deformed target leads to quasi-fission and collision with the sides leads to fusion-fission. According to PEF theory, at sub-barrier energies the channel coupling effects shift the value of α_{BG} towards higher mass asymmetries resulting in NCN Fission events.

We are studying the fusion cross sections and fragment angular distribution of two systems, ^{13}C+^{232}Th and ^{13}C+^{235}U, for energies from below barrier to well above barrier with the objective of investigating:

1. The effect of target projectile mass asymmetry on the fusion-fission process. The measured anisotropy values will be compared with SSPM predictions and the deviations provide a measure of contributions from NCN Fission. Fragment Angular Distribution of ^{13}C+^{232}Th having mass asymmetry α = .89 will be measured and compared with SSPM predictions. Earlier studies have shown that ^{12}C+^{232}Th, α = 0.90 results are in agreement with SSPM at above barrier energies and ^{14}N+^{232}Th, α = 0.886 system shows deviations. The present study will give the value of α at which the NCNF events become significant.

2. Since ^{232}Th is a deformed target, anomalous anisotropy values are expected at near barrier energies. It has been reported earlier that this anomaly is somewhat reduced by non-zero target spins [Lestone 1997] and projectile spins [Nayak 2000]. The near and below barrier results using ^{13}C (spin = 1/2) projectile will be compared with that of ^{12}C (spin zero), from the literature, to look for any effect resulting from the non-zero projectile spin.

3. The angular distribution of fragments from the ^{248}Cf compound nucleus has been studied earlier with different entrance channels mass asymmetries, using ^{11}B+^{237}Np, ^{12}C+^{236}U and^{16}O+^{232}Th systems [Kailas 1999, Vandenbosch 1996]. It was reported that the effect of entrance channel mass asymmetry vanishes at sufficiently higher energies. This aspect will be investigated again with ^{13}C+^{235}U reaction, that also results in the ^{248}Cf compound nucleus.

4. For deformed actinide targets with zero spin, the anisotropy plot shows a bump at the barrier. The washing out of this bump for targets having large ground state spin has been reported by Lestone [Lestone 1997] for the ^{12}C+^{235}U system. We will study this effect by comparing the results of ^{13}C projectile on ^{232}Th (zero spin) and ^{235}U (spin = 7/2) targets.

5. The compound nucleus angular momentum values are calculated from the measured fission cross sections for both the systems and the same

is used for calculating the anisotropy values using SSPM theory. SSPM and PEF model calculations are performed for both systems and the results are compared.

A brief description of the fusion-fission theory is given in chapter two along with relevant experimental results from the literature. Chapter three explains the experimental setup that is more or less common for both the systems. In chapter four we present the study of the ^{13}C+^{232}Th system. The experimental procedure, results obtained and their comparison with the theoretical model calculations are given. Chapter five explains the experiment, results obtained and the model calculations for the ^{13}C+^{235}U system. In chapter six, we discuss results and conclude.

Bibliography

[Back 1985]	Back B B et al, Phy. Rev. C Vol. 32 (1985)
[Beckerman 1988]	Beckerman M, Rep. Prog. Phy. 51(1988)
[A Bohr 1956]	Bohr A (1956) Proc. U.N. Int. Conf. Peaceful Uses of At. Energy Vol 2. p151
[Bohr 1936]	Bohr N, Nature 137 (1936)
[Bohr 1939]	Bohr N, Phy. Rev. Vol 56(1939)
[Businaro 1955]	Businaro U L et al, IL Nuovo Cimento, Vol. I.N.4 (1955)
[Dasgupta 1998]	Dasgupta M et al, Annu. Rev. Nucl. Part. Sci. (1998)401-61
[Dasso 1983]	Dasso C H, S. Landowne and A. Winther, Nucl. Phys. A407, 221 (1983)
[Halpern 1957]	Halpern I and Strutinsky V M, Proc. of Second United Nations International Conference on the Peaceful Uses of Atomic Energy, Geneva (1957)
[Hinde 1995]	Hinde D J et al, Phy. Rev. Let Vol 74(1995)
[Kailas 1999]	Kailas S et al, Phy Rev C Vol 59(1999)

[Kailas 1997]	Kailas S, Phy. Rep. 284(1997) and references sited
[Krappe 1979]	Krappe H J et al, Phy. Rev. C Vol. 20(1979)
[Nayak 2000]	Nayak B K et al, Phy Rev C Vol 62(2000)
[Lestone 1997]	Lestone J P et al, Phy. Rev. C Vol 56(1997)
[Ramamurthy 1985]	Ramamurthy V S et al, Phy. Rev. Lett. 54(1985)
[Vandenbosch 1996]	Vandenbosch R et al, Phy Rev C Vol 54 (1996)
[Vandenbosch]	Vandenbosch R, Huizenga J R, Nuclear Fission, Academic Press, 1973
[Vaz 1978]	Vaz L C et al, Phy. Rev. C Vol. 18(1978)

Investigation of Fusion Reactions of Heavy Ions And Development of Necessary Instrumentation

A Thesis submitted to the University of Calicut
for the partial fulfillment of the requirements
for the degree of
Doctor of Philosophy in Physics

Ajith Kumar B.P.

Department of Physics
University of Calicut
May, 2007

Chapter 2

Understanding Heavy Ion Fusion-Fission

When a projectile and target come close together they form a combined system in which the nucleons interact strongly with each other. Except for very light systems the energy carried in by the entrance channel is shared more or less stochastically among many configurations. Once this happens it takes a long time, on a nuclear scale, until the energy is concentrated again in some configuration of nucleons from which a transition to an open final channel can take place. It is postulated that in such cases the fusion reaction proceeds through the formation of an intermediate compound nucleus that decays later into true final channels. The probability of formation of the compound nucleus, called the fusion cross section, is estimated experimentally by measuring the total rate of decay into the final products. By observing various properties of the decay products, the validity of the assumption of compound nucleus can be verified.

We require a theoretical framework to explain the experimental observables like fusion cross sections and the spin distributions in terms of certain interaction potentials and reaction mechanisms. *The one dimensional potential barrier formed by the long range repulsive Coulomb and the short range attractive nuclear interactions can be taken as a starting point to explain the fusion mechanism.* This simple model is refined further by adding quantum tunneling, channel coupling etc. to explain the observed experimental fusion cross sections and other observables.

2.1 The one Dimensional Potential Barrier model

The potential experienced by the projectile when it approches the target nucleus is shown in figure 1.1. The potential is a function of the radial distance between the two nuclei but the angular momentum of the compound nucleus formed after collision depends on the impact parameter. The $\ell = 0$ curve represents a head-on collision and the higher ℓ values are for larger impact parameters. The effect of angular momentum can be taken into account by modifying the interaction potential as explained below [L.I.Schiff].

The time independent Shrodinger equation for the motion of a particle of mass m in a spherically symmetric potential $V(r)$ can be written in spherical polar coordinates as:

$$\frac{-\hbar^2}{2m}\left[\frac{1}{r^2}\frac{\partial}{\partial r}\left(r^2\frac{\partial}{\partial r}\right)+\frac{1}{r^2\sin\theta}\frac{\partial}{\partial\theta}\left(\sin\theta\frac{\partial}{\partial\theta}\right)+\frac{1}{r^2\sin^2\theta}\frac{\partial^2}{\partial\phi^2}\right]u+V(r)u=Eu \tag{2.1}$$

This equation can be separated into radial and angular parts. The radial part of the wave equation

$$\frac{1}{r^2}\frac{\partial}{\partial r}\left(r^2\frac{\partial R}{\partial r}\right)+\left\{\frac{2m}{\hbar^2}\left[E-V(r)\right]-\frac{\ell(\ell+1)}{r^2}\right\}R=0 \tag{2.2}$$

can be re-written as

$$\frac{\hbar^2}{2m}\frac{d^2\chi}{dr^2}+\left[V(r)+\frac{\ell(\ell+1)\hbar^2}{2mr^2}\right]\chi=E\chi \tag{2.3}$$

by substituting $R(r)=\chi(r)/r$. Thus the radial motion is equivalent to the one dimensional motion of a particle in a potential with the addition of an extra term to the potential. If we put $L=\hbar\sqrt{\ell(\ell+1)}$ it can be seen that the additional term added to the potential corresponds to centrifugal potential associated with the angular momentum. In classical terms the angular momentum L of a particle orbiting with an angular velocity ω at a radius r is given by $L = mr^2\omega$ and the centrifugal force is given by $mr\omega^2$. This force is equal to the derivative of the centrifugal potential term added to the radial potential.

$$-\frac{d}{dr}\left(\frac{\ell(\ell+1)}{2mr^2}\right) = -\frac{d}{dr}\left(\frac{L^2}{2mr^2}\right) = \frac{L^2}{mr^3} = mr\omega^2. \tag{2.4}$$

From figure 1.1 it can be seen that the potential possesses an outer maximam, termed as the fusion barrier, at a radial separation where the Coulomb and short range nuclear forces just cancel out. At smaller separation there is an attractive pocket in the potential that enables fusion. The centrifugal potential increases the barrier heights, slightly shifts the barrier locations and reduces the depth the potential pocket, required for the formation of a compound nucleus. At certain maximum values of $\ell = \ell_{crit}$ the pocket vanishes and that sets a limit on the maximum angular momentum of the compound nuclues formed.

2.2 Calculating the Fusion Cross Section

Since we assume that the two nuclei fuse together once they overcome the ion-ion potential barrier, the fusion cross sections should follow from the transmission probabilities through the barrier. Comparing the results with measured cross sections will verify the validity of the one dimensional potential barrier model. The ion-ion potential is given by equation

$$V_\ell(r) = V_N(r) + V_C(r) + \frac{\hbar^2\ell(\ell+1)}{2\mu r^2} \tag{2.5}$$

where V_N is the nuclear potential, V_C the Coulomb potential and μ is the reduced mass of the system. The transmission probability as function of energy should be calculated for all possible ℓ values. Due to the quantum tunneling the transmission probabilities at sub-barrier energies are non-zero and can be evaluated using the WKB approximation. The action integral $S_\ell(E)$ and transmission coefficient $T_\ell(E)$ are given by the following relations

[Balantekin 1998]

$$S_\ell(E) = \sqrt{\frac{2\mu}{\hbar^2}} \int_{r1\ell}^{r2\ell} \left[V_\ell(r) - E\right]^{1/2} dr \tag{2.6}$$

$$T_\ell(E) = \{1 + exp[2S_\ell(E)]\}^{-1} \tag{2.7}$$

where the limits of integration are the classical turning points for the ℓth partial wave. The fusion cross sections for each partial wave is given by

$$\sigma_\ell(E) = \frac{\pi\hbar^2}{2\mu E}(2\ell + 1)T_\ell(E) \tag{2.8}$$

The total fusion cross section is obtained by summing over all partial waves below ℓ_{crit}as shown below.

$$\sigma(E) = \sum_{\ell=0}^{\ell_{crit}} \sigma_\ell(E) \tag{2.9}$$

The computation of $\sigma(E)$ in terms of the potential given by 2.5 is very tedious due to the complex nature of the nuclear potentials but the transmission coefficients can be calculated analytically for some simplified barrier shapes. If we assume the shape of the barrier is an inverted parabola, the Coulomb plus nuclear part of the potential can be replaced by an inverted harmonic oscillator potential giving

$$V_\ell(r) = V_0 - \frac{1}{2}\mu\omega_0^2(r - r_0)^2 + \frac{\hbar^2\ell(\ell + 1)}{2\mu r^2}. \tag{2.10}$$

The transmission coefficients for the above potential is given by the Hill-Wheeler formula [Hill, Wheeler 1953]

$$T_\ell(E) = \left\{1 + \exp\left[\frac{2\pi}{\hbar\omega_\ell}(V_\ell - E)\right]\right\}^{-1} \tag{2.11}$$

where V_ℓ denotes the barrier height of the ℓ^{th}partial wave and $\hbar\omega_\ell$ the corresponding barrier curvature. There are several potentials like the proximity potential, generalized liquid drop potential etc. [Krappe 1979] that have been widely used to interpret the experimental data [Beckerman 1981]. A simple expression for total fusion cross section can be obtained if the barrier positions and curvatures are assumed to be independent of angular momentum.

$$\hbar\omega_\ell = \hbar\omega_0 \ ; \ \ V_\ell = V_0 + \frac{\hbar^2 \ell(\ell+1)}{2\mu r_0^2} \tag{2.12}$$

The total cross section can then be obtained by inserting equations 2.11 and 2.12 into 2.8 and integrating to obtain the Wong formula for total fusion cross section. [Wong 1973]

$$\sigma(E) = \frac{\hbar\omega_0 r_0^2}{2E} \ln \left[1 + \exp\left[\frac{2\pi}{\hbar\omega_0}(E - V_0)\right]\right] \tag{2.13}$$

At energies well above barrier, $E >> V_0$, expression 2.13 reduces to the classical formula for the capture of the charged particle by the nucleus;

$$\sigma(E) = \pi r_0^2 (1 - \frac{V_0}{E}) \tag{2.14}$$

For small values of the expression reduces to the exponential relation

$$\sigma(E) = (r_0^2 \hbar\omega / 2E) e^{[2\pi(E - V_0)/\hbar\omega_0]}. \tag{2.15}$$

According to equation 2.14 $\sigma(E)$ Vs $1/E$ plot should be a straight line. The experimental data for ^{74}Ge + ^{74}Ge [Beckerman 1988]are shown is figure 2.1. It can be seen that there is a departure from the linear dependency at sub-barrier energies where the quantum tunneling effect come into the picture.

2.3 Limitations of the One Dimensional Barrier Model

The one dimensional barrier penetration model successfully explained the fusion cross sections of the light nuclei. However, the observed cross sections for heavy nuclei at sub-barrier energies are found to be much larger than the predictions. Measurements for ^{16}O + ^{144,148,154}Sm [Leigh 1993] showed enhanced

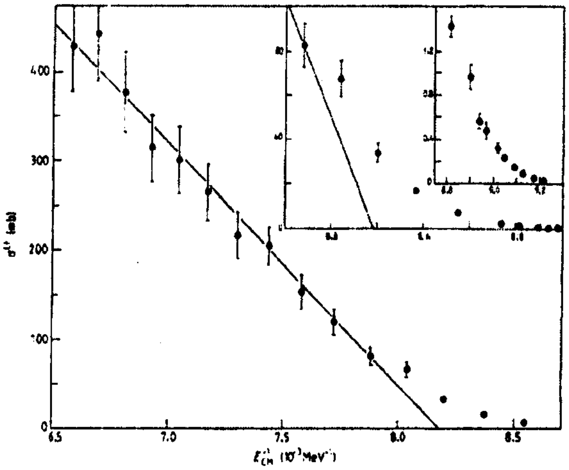

Figure 2.1: Fusion cross sections for $^{74}Ge + ^{74}Ge$ as a function of the inverse of the center of mass energy. The insert shows an expanded view of the sub-barrier region ([Beckerman 1988])

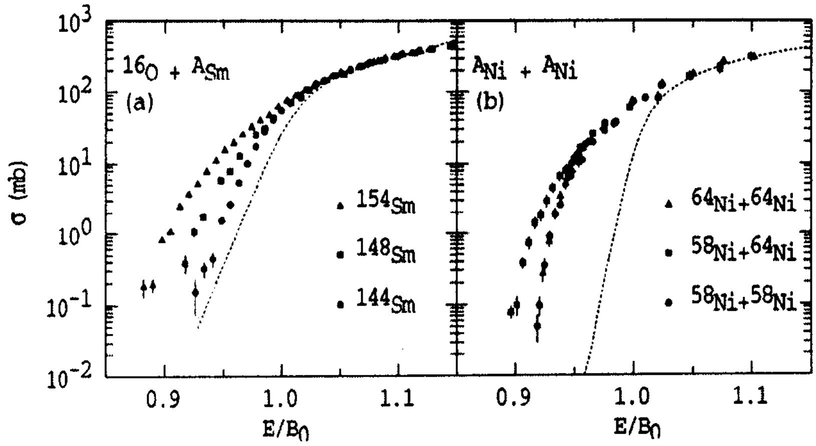

Figure 2.2: Fusion excitation functions for ^{16}O on Sm isotopes with different deformations. Cross sections for^{58}Ni+^{58}Ni,^{58}Ni+^{64}Ni and ^{64}Ni+^{64}Ni depends on the transfer reaction Q-values.

sub-barrier cross section that increases with neutron number, see figure 2.2. This disagreement could happen either due to the usage of incorrect barrier or due to the failure of the model itself. This aspect was investigated by Balantekin and Koonin ([Balantekin 1983]) using an inversion procedure to deduce the barrier thickness from the measured fusion cross section data. The thickness of the barrier is the difference between the limits of the action integral

$$S_\ell(E) = \sqrt{\frac{2\mu}{\hbar^2}} \int_{r1\ell}^{r2\ell} \left[V(r) - E + \frac{\ell(\ell+1)\hbar^2}{2\mu r^2} \right]^{1/2} dr \tag{2.16}$$

and are determined by the zeros of the integrand. In order to get an analytic solution it is supposed that for a given E the angular momentum dependency can be reproduced by shifting the energy as shown below.

$$T_\ell(E) = T_0\left(E'\right) \quad where\ E' = \left[E - \frac{\ell(\ell+1)\hbar^2}{2mr^2(E)} \right] \tag{2.17}$$

Applying this to the equation 2.9 and converting it to an integral we get

$$E\sigma(E) = \pi r^2(E) \int_{-\infty}^{E} dET(E). \tag{2.18}$$

The relation between $S_0(E)$ and $\sigma(E)$ can be written as

$$S_0(E) = \frac{1}{2} \ln \left\{ \left[\frac{d}{dE} \left(\frac{E\sigma}{\pi r^2} \right) \right]^{-1} - 1 \right\} \tag{2.19}$$

Thus S_0 is completely determined by the measured cross sections assuming the value of r equal to the radius of the barrier. Inverting the action integral provides the barrier thickness

$$t(V) = r_2(V) - r_1(V) = -\frac{2}{\pi}\sqrt{\frac{\hbar^2}{2m}} \int_V^B \frac{dS_0/dE}{\sqrt{E-V}} dE \tag{2.20}$$

If we substitute $S_0(E)$ from equation 2.20 to 2.19 it can be seen that the the barrier thickness is obtained by a double differentiation of the term $E\sigma(E)$. The inversion method assumes the existence of a single potential barrier. Calculations were carried out by Balantekin et al. [Balantekin 1983]

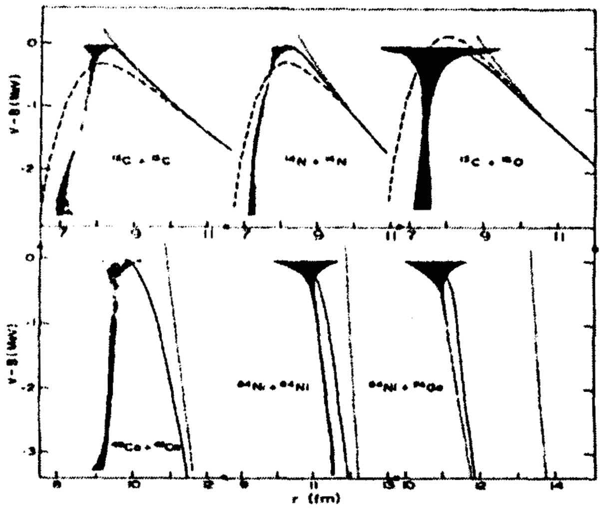

Figure 2.3: Effective one dimensional potential extracted from the fusion cross section data using the inversion technique. For the lighter systems the potentials are similar to the phenomenological KNS potential [Krappe 1979]. The ^{40}Ca + ^{40}Ca potential is very narrow. For heavier systems the thickness functions are inconsistent with the assumption of a single valued one dimensional potential.[Balantekin 1983]

for several systems. The results matched with phenomenological potentials for lighter systems but the heavier systems failed to give a single valued one dimensional potential as shown in figure 2.3. *This indicates that the deviations are not due to the usage of wrong potential but the assumption of two inert spherical nuclei interacting through a one dimensional potential itself is not realistic.* This resulted in investigating the role played by the internal degrees of freedom, like rotation, surface vibrations etc., of the target and projectile nuclei in the fusion process.

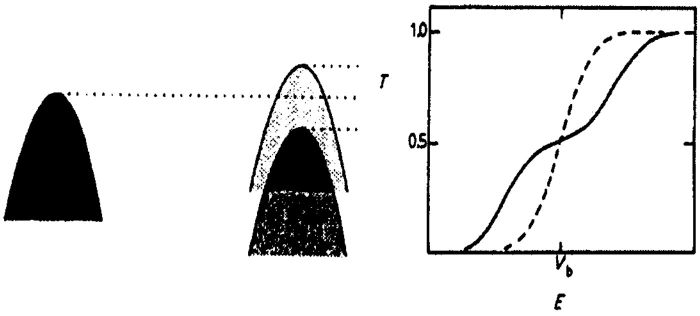

Figure 2.4: Bifurcation of potential barrier by coupling interaction. The broken curve gives the transmission through the unmodified barrier and the solid curve through the modified barrier.

2.4 Effects of Internal Structure and Barrier distributions

The effect of the coupling of the translational motion to the intrinsic degrees of freedom can be qualitatively explained in the following manner. In the uncoupled case the incoming flux sees a single barrier of some fixed height. The coupling with intrinsic degrees of freedom has the effect of modulating the height of this barrier. That implies a spectrum of barriers whose heights are around the original barrier height. The total fusion cross section will be decided by a weighted average of all the barriers. Due to the exponential dependency of sub-barrier cross section on the barrier height, any spread in the height leads to a cross section enhancement. The increase in transmission due to the contributions from the lower barriers will compensate more than the decrease caused by the higher barrier heights. Barrier distribution due to static deformation can be visualized as the encounter of the incoming nuclei at different orientations.

2.4.1 Coupled Channel Theory

Effect of nuclear intrinsic degrees of freedom on fusion cross section can be studied theoretically by solving the coupled channels equations that determine the wave functions of relative motion numerically. The number of channels can be reduced by ignoring the change of centrifugal potential barrier due to the nuclear intrinsic excitation. Further if we ignore the finite excitation energy of nuclear intrinsic motion the coupled channel equations can be decoupled into a set of single eigenvalue equations. Study done by Dasso et al [Dasso 1983] assumed a constant coupling and obtained the decoupled equations that could be solved with less difficulty. The starting point of the constant coupling model is a set of coupled Schrodinger equations:

$$\left(-\frac{\hbar^2}{2\mu}\frac{d^2}{dr^2} + V(r) - E\right) u_\alpha(r) = \sum \langle\alpha|H_0 + V^c|\beta\rangle\, u_\beta(r) \tag{2.21}$$

where H_0 is the intrinsic Hamiltonian and $|\beta\rangle$ are the associated eigen vectors $H_0\,|\beta\rangle = \varepsilon_\beta\,|\beta\rangle$. V^c is the coupling interaction. The equations may be decoupled if V^c factors into relative and intrinsic parts and is spatially constant in the vicinity of the barrier. The eigenvalues λ_β of $H_0 + V^c$ describing the interacting intrinsic system are obtained by diagonalizing the matrix

$$M_{\alpha\beta} = \langle\alpha|\, H_0 + V^c\, |\beta\rangle = \delta_{\alpha\beta\varepsilon\beta} + F_0 V_{\alpha\beta}. \tag{2.22}$$

The decoupled Schrodinger equation is

$$\left(-\frac{\hbar^2}{2\mu}\frac{d^2}{dr^2} + V(r) + \lambda_\beta - E\right) v_\beta = 0 \tag{2.23}$$

and the total transmission coefficient is

$$T = \sum_\beta |\langle 1|\beta\rangle|^2\, T\left(E, V(r) + \lambda_\beta\right) \tag{2.24}$$

The eigenvalues λ_β represents the coupling strengths. *The incident flux sees a spectrum of barriers $V(r) + \lambda_\beta$ instead of a single barrier.* The bifurcation of the potential barrier and the effect of it on the transmission probability for coupling with one intrinsic degree of freedom is shown schematically in figure 2.4 [Beckerman 1988]. The total transmission is the sum of the transmission coefficients of each barrier weighted by the overlap factor $|\langle 1|\beta\rangle|^2$

between the entrance channel and the corresponding intrinsic channel.

2.4.2 Barrier Distribution as Tool to Study Fusion

The barrier distribution $D_{exp}(E)$ is obtained from the fusion cross sections by taking its second derivative using the three point difference formula

$$\frac{d^2(\sigma E)}{dE^2} = \left(\frac{(E\sigma)_3 - 2\,(E\sigma)_2 + (E\sigma)_1}{\Delta E^2}\right) \tag{2.25}$$

where E_1, E_2 and E_3 are three discrete energies and $\Delta E = (E_2 - E_1) = (E_3 - E_2)$ .The extraction of barrier distributions from experimental fusion cross sections are found to be a valuable tool in understanding the fusion process. The role of various internal degrees of freedom could be verified by comparing the resulting barrier distributions with the ones extracted from experimental fusion cross sections. Unlike the fusion cross section plot, the barrier distribution $D_{exp}(E)$ clearly shows the difference in the structure of different compound nuclei. Figure 2.5 shows the barrier distributions extracted from the measured fusion cross sections for several systems.

2.5 Decay of Compound Nucleus

Even though we could conceptually define the fusion process in terms of a barrier penetration picture, the experimental observables are the decay products of the compound nucleus. They depend on the fusion potential as well on the subsequent evolution of the system. After getting captured in the fusion potential some mass flow occurs to form a neck and the system comes to thermal equilibrium. At this point the composite system can be called a di-nucleus, that may proceed towards a fully equilibrated compound nucleus or undergoes fission. After relaxing all but the shape degrees of freedom, they can be called inside the fission potential.

For light nuclei the shape evolution inside the fission potential leads to the compound nucleus at its equilibrium deformation, which decays by emitting light particles like protons, neutrons, alphas etc. and this process is

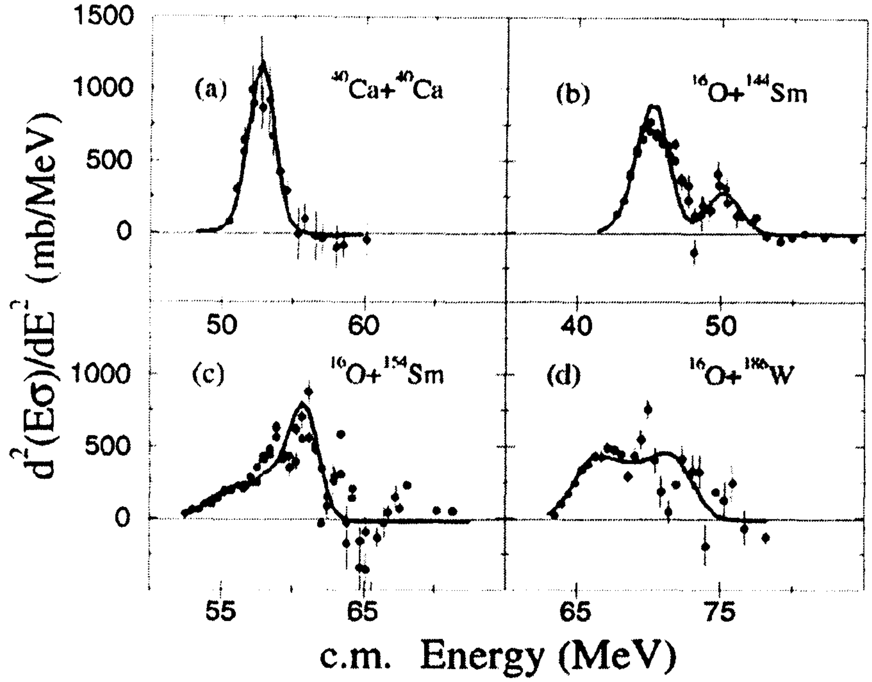

Figure 2.5: Experimental fusion barrier distributions for different systems. (a) ^{40}Ca + ^{40}Ca shows a single barrier and implies absence of coupling. This is expected from the double closed-shell nature of the nuclei. (b) ^{16}O + ^{144}Sm shows a second bump due to the coupling to some excited states of the target nucleus. (c) ^{16}O + ^{154}Sm shows a gradual increase on the low energy side of the un-coupled barrier. This implies a deformed target. (d) ^{16}O + ^{186}W also implies a deformed target with a negative values for the deformation parameter β_4 as opposed to the positive β_4 for the ^{154}Sm target.

called evaporation. The remaining residual nucleus is called the evaporation residue. The evaporation process is generally accompanied by emission of γ-rays. For heavy systems the prominent mode of decay is fission where the compound nucleus splits into two halves of more or less equal size. The fission process is accompanied by emission of light particles and γ-rays. For intermediate masses these two processes compete each other. Since both the systems investigated in this thesis, ^{232}Th + ^{13}C and ^{235}U + ^{13}C, decay mainly through fission, the theory of fission will be discussed in some detail.

The statistical theory of fission gives the following picture. The energy brought in by the incoming projectile, kinetic as well as the released binding energy, is distributed stochastically among all the nucleons. At this point the various processes like evaporation and fission start competing each other. The probability of taking a particular route depends on the density of final levels in each case. If the internal energy happens to concentrate on the deformation modes that lead to the saddle point shape, fission can occur, again as a function of the density of levels of the saddle point.

2.6 Nuclear Fission

Fission was discovered by Otto Hahn and Fritz Strassman [Hahn 1939] in 1938 . They found that irradiating uranium with neutrons results in ligher products like barium, lanthanum etc. Fission has acquired a unique importance among nuclear reactions due to its applications in the field of energy and weapons. From the point of view of basic research, fission is interesting in its own right as a large scale collective motion of the nucleons, as an important exit channel for many nuclear reactions, and as a source of neutron-rich nuclei for nuclear structure studies and for generating radioactive ion beams (RIB). It has been observed that heavy nuclei, actinides and above, undergo spontaneous fission with measurable probability. Most of the nuclei undergo fission if bombarded with gamma rays, nucleons or heavy ions. The probability of fission is found to be a function of the excitation energy. Fission process is generally accompanied by the emission of neutrons and gamma rays. Fission half-lives, their dependency on the excitation energy, mass, charge and angular distribution of the fission fragments, properties of the emitted neutrons and gammas etc. are studied to gain some understanding about the mechanism of fission process. The fission-fragment angular distribution has been found to be a rich source of information about the compound nucleus formation and the fusion-fission process. Studies show that it can be related to the evolution of the composite system that relaxes in mass, energy, angular momentum and shape degrees of freedom, the viscous nature of the nuclear matter and the entrance channel effects. Study of fragment angular distributions also helps in understanding the non-equilibrium modes of fission like fast fission, quasi-fission and pre-equilibrium fission where some of the internal degrees of freedom are not fully equilibrated.

While we understand many aspects of the fission process, till date there is no overall theoretical framework that gives a satisfactory explanation for all the observations. The liquid drop model [Bohr 1939] has been successful in describing the general features of the fission. The potential energy as a function of deformation calculated using the liquid drop model exhibits a barrier that has to be overcome by the compound nucleus in order to undergo fission. This model could account for the energy release during fission, the dependence of fission probability on excitation energy and several other aspects. The simple liquid drop model was further modified to include the shell and single particle effects to explain most of the experimental observations.

2.6.1 The Liquid drop model

The preliminary aspects of the fission process can be explained by comparing the fissioning compound nucleus to a charged liquid drop. The excitation energy available to the nucleus causes shape oscillations. As it deforms from the spherical shape the Coulomb repulsion energy decreases due to the larger average separation between protons but the nuclear surface energy increases due to the increased surface area. The deformation at which these two changes balance each other is called the *saddle point* shape. Once the compound nucleus deforms beyond the saddle point it is committed to fission. When it happens the neck between the nascent fragments disappears within

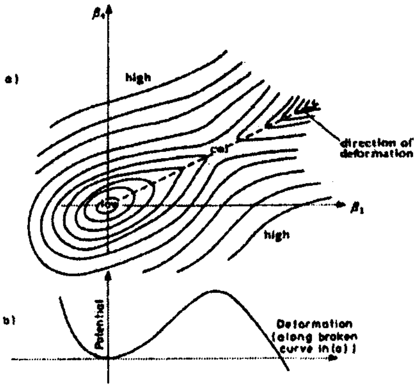

Figure 2.6: (a)Potential energy contours of a fissionable nucleus as function of the quadrupole and hexadecapole deformation parameters.(b) Potential energy along the minimum energy trajectory for increasing elongation.

a short time and the nucleus divides into two deformed fragments touching each other, which is called the *scission point*. The large Coulomb repulsion between them is converted into their kinetic energies. As they move away the deformed fragments contract to more spherical shapes, converting their potential energy of deformation into internal excitation energy. This results in the emission of *prompt neutrons* and gamma rays. On a larger timescale the neutron rich fragments undergo β decay.

Several aspects of fission can be explained by studying the total potential of the fissioning system as a function of deformation. Deformations of the nucleus from spherical shape can be parameterized using the relation

$$R(\theta) = R_0\left(1 + \alpha_0 + \alpha_2 P_2(\cos\theta) + \cdots\right) \tag{2.26}$$

where α_n are the deformation parameters and P_n the Legendre polynomials. We treat the nucleus as an incompressible liquid drop of volume $(4\pi/3)R_0^3$, where $R_0 = r_0 A^{\frac{1}{3}}$, uniformly charged with a total charge Ze, and having a surface tension O. The surface energy plus the electrostatic energy is given by [Bohr 1939]

$$E_{S+E} = 4\pi r_0^2 A^{\frac{2}{3}} O \left[1 + \frac{2\alpha_2^2}{5} + \frac{5\alpha_3^2}{7} + \cdots\right] + \frac{3(Ze)^2}{5r_0 A^{\frac{1}{3}}} \left[1 - \frac{\alpha_2^2}{5} - \frac{10\alpha_3^2}{49} + \cdots\right] \tag{2.27}$$

The potential energy as a function of deformation parameters is shown in figure 2.6 . For small spheroidal deformations α_4 can be ignored and distortion energy can be written in terms of α_2 and equating the surface and Coulomb terms provides a critical value for Z^2/A beyond which the nucleus is not stable with respect to small deformations. Equating the coefficients of α_2 gives:

$$\frac{3Z^2e^2}{5r_0 A^{\frac{1}{3}}} \frac{\alpha_2^2}{5} = 4\pi r_0^2 A^{\frac{2}{3}} O \frac{2\alpha_2^2}{5} \tag{2.28}$$

$$\Rightarrow \left(\frac{Z^2}{A}\right)_{critical} = 10 \left(\frac{4}{3}\pi r_0^3\right) \frac{O}{e^2} \tag{2.29}$$

Let E_S^0 and E_C^0 are the surface and Coulomb energies for zero deformation. The drop will become unstable at the deformation where ΔE_C exceeds ΔE_S, or when $E_C^0/2E_S^0 = 1$. The fissionability of a nucleus is defined in terms of a parameter called fissility

$$x = \frac{E_C^0}{2E_S^0} = \left(\frac{Z^2}{A}\right) / \left(\frac{Z^2}{A}\right)_{critical} \tag{2.30}$$

The deformation parameters corresponding to the saddle point give us the critical form of the drop, and the potential energy required for this distortion is called the critical energy of fission E_f. Bohr derived the relation between the fissility and the critical energy:

$$E_f = 4\pi r_0 O A^{\frac{2}{3}} \left[\frac{98}{135}\left(1 - x^2\right) - \frac{11368}{34425}\left(1 - x^4\right) + \cdots\right] \tag{2.31}$$

and calculated $(Z^2/A)_{critical}$ from the critical energy and and fissility of uranium isotopes. Assuming E_f= 6 MeV and $x = 0.74$ for ^{239}U, $(Z^2/A)_{critical} = (92)^2/239 \times 0.74 = 47.8$. From this the fissility of other nuclei can be calculated. The parameters Z^2/A and x provides measures of the relative fissionability of the nuclei. For example, highly fissionable nuclei like ^{239}Pu have a Z^2/A value of 36.97 while the less fissionable ^{209}Bi has a Z^2/A of 32.96. According to the liquid drop model, nucleus with fissility value greater than unity cannot exist since they undergo fission instantaneously. The fission rates at excitation energies below the barrier are decided by the penetration probabilities. Assuming a harmonic oscillator potential the transmission coefficient is given by the Hill-Wheeler formula

$$T = \{1 + \exp\left[2\pi\left(E_F - E\right)/\hbar\omega\right]\}^{-1} \tag{2.32}$$

where E_F is the fission barrier height and E is the available excitation energy (compare with equation 2.11). The parameter $\omega = \sqrt{C/B}$ where C is the curvature of the potential barrier and B is the effective inertia of the fissioning system. Even though the liquid drop model could explain some of the features of fission further experimental results revealed the complexity of fission process and the inadequacy of this simple model. The observed fission fragment mass asymmetry, non-spherical ground state of several heavy nuclei, discrepancy between the observed and calculated spontaneous fission life times and the discovery of short lived fission isomers prompted modification of the simple LDM.

Most of the spontaneously fissioning nuclei splits asymmetrically with a roughly constant heavy fragment mass near $A = 140$ as shown in figure 2.7. For ^{252}Cf the fragment mass distribution shows a peak to valley ratio of 750. The fermium isotopes exhibit a change in mass asymmetry with mass number as shown in figure 2.8 [Flynn 1975]. The trend is towards more symmetric fission as the mass number increases. The total kinetic energy of fragments is found to be higher for symmetric fission. In the case of induced fission the probability of symmetric fission increases with excitation energy. The possibility of a uniformly charged liquid drop having modes of shape oscillations leading to asymmetric fission was explored and the answer was found to be negative. [Frankel 1947].

For nuclei in the actinide region, with fissility values slightly less than unity, the fission barrier between the ground state shape and the separated fragment configuration is sufficiently low and spontaneous fission due to

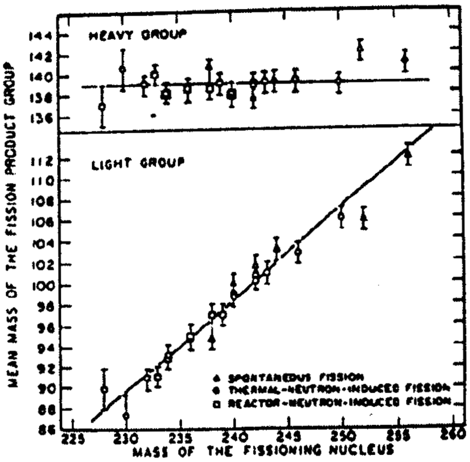

Figure 2.7: Average masses of the heavy and light fragments as a function of mass number. [Flynn 1972]

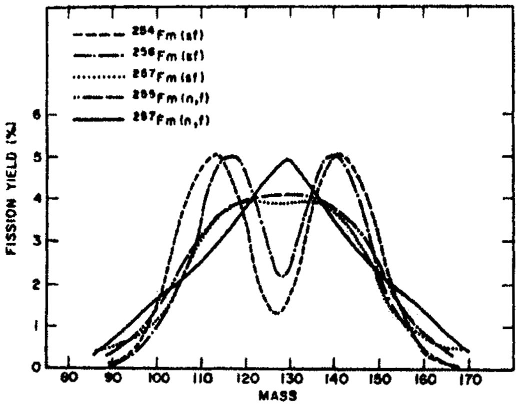

Figure 2.8: Fission of fermium isotopes shifts towards more symmetric as the mass increases. The tendency towards symmetric fission with excitation energy is evident from the neutron induced fission of ^{255}Fm and ^{257}Fm.

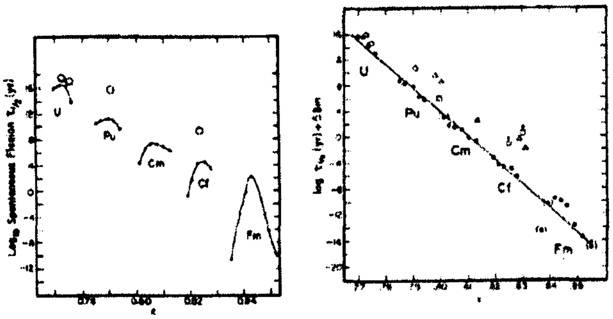

Figure 2.9: (a) Spontaneous fission half lives as a function of fissility. (b) Corrected half lives by applying the deviation of the ground state masses δ_m from the liquid drop model values. •even-even ∘ even-odd◁odd-even

quantum tunneling occurs with measurable probability. According to the liquid drop model the height of the barrier reduces with increasing fissility and we expect a smooth correlation between spontaneous fission half lives and fissility. However measured half lives shows different kinds of deviations. For a given element isotopes with larger number of neutrons are expected to have longer life times due to the smaller Z^2/A values. Experimental results show the half lives of even-even isotopes of a given element decreases with mass number as shown in figure 2.9. For example ^{256}Fm has a much shorter haf-life than ^{254}Fm contrary to the LDM prediction. This has been explained on the basis of the deviations of ground state masses of nuclei from the smooth liquid drop prediction due to the shell effects. After applying this mass correction δ_m, the half-lives shows better agreement with the fissility values, figure 2.9. The discovery of spontaneously fissionable isomers was another phenomena that could not be explained by LDM. The fissionable isomers have been produced using reactions like $(d, 2n)$, (d, p) etc. and they show half lives of the order of nanoseconds [Britt 1971].

2.6.2 Refinements to LDM, Strutinsky Hybrid Model

The liquid drop model assumes a uniform distribution of charge to calculate the Coulomb repulsion and a well defined smooth surface to calculate the surface tension. It is well established that the nuclear properties like binding energy, stability, isotopic abundance etc. shows remarkable regularities when number of neutrons or protons are equal to 2, 8, 20, 28, 50 or 82, [Mayer 1950] referred to as the magic numbers. This also implies that the effect of shell structure need to be included in the potential energy calculations to get realistic results. Even before the mathematical formulation of nuclear shell model with spin-orbit coupling, Mayer [Mayer 1948] suggested that the asymmetric fission of ^{235}U could be due to the tendency to form a fragment with around 50 protons and 82 neutrons. Methods to include the single particle effects into the macroscopic liquid drop model were attempted and in 1967 Strutinsky developed a method to include the shell and single particle effects as a correction term in to the liquid drop model.

Under Strutinsky's [Strutinsky 1967] method the shell correction was calculated by summing the energies of occupied single particle Nilsson orbitals in a potential well of given deformation and subtracting from this the energy calculated by integrating over a suitably averaged single particle level density. In other words, the shell correction δU is be treated as the difference between the total energies calculated using two different energy level schemes; one a realistic shell model energy spacings and another a 'uniform' distribution.

$$\delta U = U - \tilde{U} = \sum_{v} 2E_v n_v - 2\int_{-\infty}^{\tilde{\lambda}} E\tilde{g}(E)dE \qquad (2.33)$$

where E_v represents the nuclear levels in the average potential and n_v the occupation numbers. $\tilde{g}$(E) is a uniform distribution of nucleon states and $\tilde{\lambda}$ the corresponding chemical potential. This difference is then added to the liquid drop model energy. The total energy is written as the sum of the liquid drop model energy E_{LDM}, and the shell interactions δU. The dependence of the pairing strength on deformation also can be included in a similar manner.

$$E = E_{LDM} + \sum_{p,n} \delta U \qquad (2.34)$$

Calculations based on this corrected potential energy, as a function of deformation, explained non-spherical ground state shapes of actinide nuclei

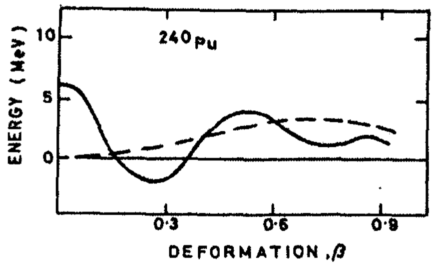

Figure 2.10: Potential energy as a function of deformation with shell correction. The dashed curve is without shell correction.

and predicted the fission barriers of the right order of magnitude. It also indicated an oscillation of the energy curve of actinide nuclei with increasing deformation as shown in figure 2.10. The double humped barrier resulting from shell corrections could explain a large number of experimental observations.

The first experimental result that could be explained on the basis of the double humped barrier was the shape isomers, having very short life times. The discovery of ^{*242}Am, with a half-life of of 14 msec, was followed by a large number of such isomeric states, mainly by isotopes of Pu, Am and Cm nuclei. The isomeric states are the nuclei trapped in the second potential well of the double humped barrier. The penetrability through the double humped barrier was calculated by Cramer [Cramer 1970] assuming two inverted parabolic wells connected by another parabolic barrier as shown in figure 2.11. The peaks in the penetrability plot explains the resonances observed in the neutron induced fission cross sections of even-even and odd-Z actinides. The barrier parameters, like the width and height, are adjusted to fit the measured fission excitation functions. One interesting observation is that assuming a reflection symmetric deformation results in an outer barrier higher than inner barrier by about 3 – 4 MeV. Experimental data on fission isomer half-lives and excitation cross sections are against this, suggesting that reflection asymmetric shape is favored energetically at the deformation corresponding the second potential well. With the recent availability of powerful computers, calculations were done to map the potential energy as a

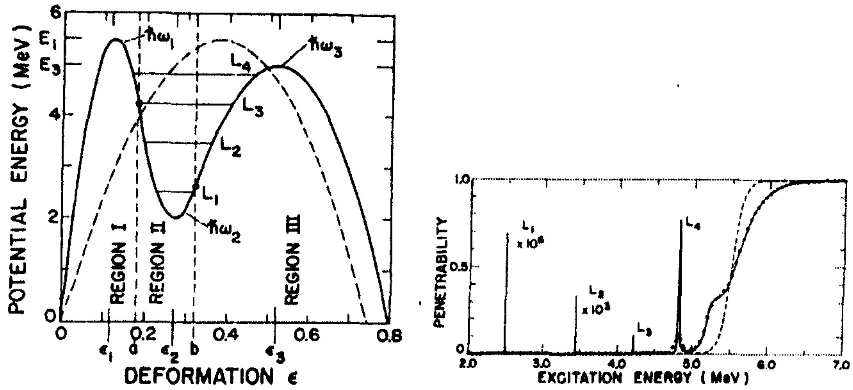

Figure 2.11: Double humped barrier approximated by three parabolic shapes for computing the penetrability analytically. The calculated penetrability shows sharp resonances at the positions of the quasi-bound levels in the outer well.[Cramer 1970]

function of shape by varying five parameters; elongation, neck diameter, deformation of two fragments and mass asymmetry [Moller 2001]. The results of calculations done for ^{228}Ra is shown in figure 2.12. These calculations confirms the role of shell effects in mass asymmetric fission and several other experimental results.

2.6.3 Fission Fragment Angular Distribution

2.6.3.1 Properties of saddle point nuclei

In 1956, A.Bohr suggested that during low energy fission most of the excitation energy goes into deformation degrees of freedom and the saddle point nucleus has a spectrum of energy levels similar to that of a normal nucleus near its ground state. This implies that the fission occurs only through few channels. Bohr formulated a simple relation between the properties of the saddle point nucleus and the fission fragment angular distribution. The total angular momentum of saddle point nucleus J , its projection along the nuclear symmetry axis K and the projection along the space fixed axis M are shown in figure 2.13. J and M are conserved quantities but K can vary during the fusion-fission process. It is reasonable to assume that the fission

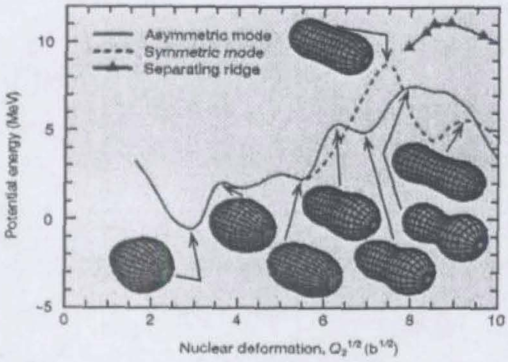

Figure 2.12: Calculated potential energy values and ridges and corresponding shapes for ^{228}Ra. Two fission paths are possible. The symmetric path has a higher saddle point and more elongated shape in the valley beyond that indicating a lower total kinetic energy for the fragments.

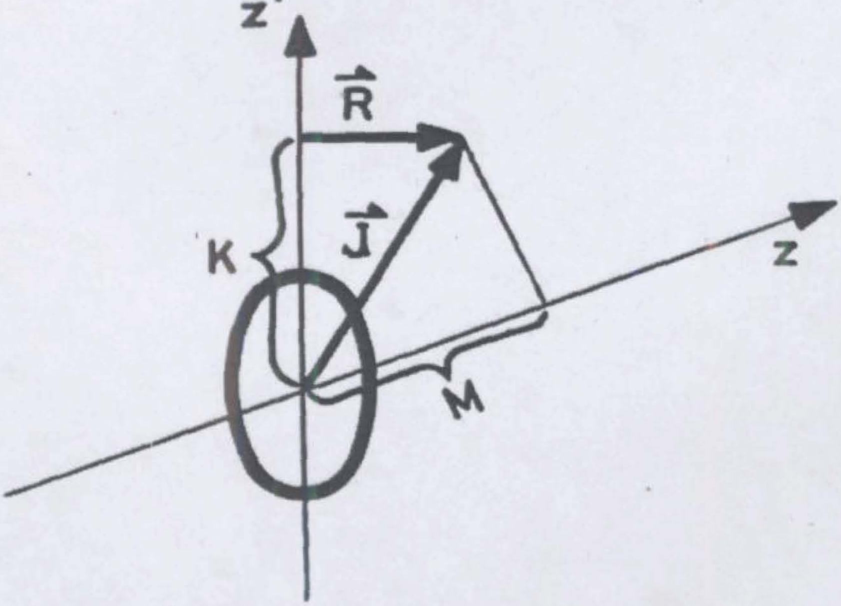

Figure 2.13: Total angular momentum J of the saddle point nucleus, its projection along the nuclear symmetry axis K and the projection along the space fixed axis (beam direction) M

fragments are emitted along the nuclear symmetry axis. If we also make the assumption that all the K mixing occurs before the compound nucleus reaches the saddle point and K does not change afterwards, it can be related to the fragment angular distribution. The probability of emitting fission fragments from a transition state with quantum numbers J, K and M at an angle θ is given by

$$P^J_{M,K}(\theta) = \frac{2J+1}{4\pi R^2} \left| D^J_{M,K}(\theta) \right|^2 2\pi R^2 \sin\theta d\theta \tag{2.35}$$

where $P^J_{M,K}(\theta)$ is the probability of emitting fragments at an angle θ into a conical volume defined by $d\theta$ and $D^J_{M,K}(\theta)$ are the symmetric top wave functions. The angular distribution $W^J_{M,K}(\theta)$ is obtained by dividing $P^J_{M,K}(\theta)$ by $\sin\theta$ as follows:

$$W^J_{M,K}(\theta) = \frac{2J+1}{2} \left| D^J_{M,K}(\theta) \right|^2 \tag{2.36}$$

Bohr pointed out that the photo-fission of even-even targets presents a simple case. The spin and parity of the even-even nucleus is 1^- and $M = \pm 1$. At excitation energies slightly above the fission barrier , the available energy is insufficient to break nucleon pair, and the energy levels of the transition nucleus are due to collective excitations. The ground state of a deformed nucleus has $K = 0$ with positive parity and even spins. The lowest lying $1-$ level is expected to have mostly $K = 0$, and the angular distribution is given by

$$W^{J=1}_{M=\pm 1,K=0}(\theta) = \frac{1}{2}(2J+1) \left\{ P_{J=1,M=+1} \left| D^1_{1,0}(\theta) \right|^2 + P_{J=1,M=-1} \left| D^1_{-1,0}(\theta) \right|^2 \right\} \tag{2.37}$$

Since the probabilities of forming a compound nucleus with the two possible values of M are same, the expression becomes

$$W(\theta) = \frac{3}{2} \left\{ \frac{1}{2} \left| D^1_{1,0}(\theta) \right|^2 + \frac{1}{2} \left| D^1_{-1,0}(\theta) \right|^2 \right\} \tag{2.38}$$

In a similar manner we can calculate the angular distribution for the

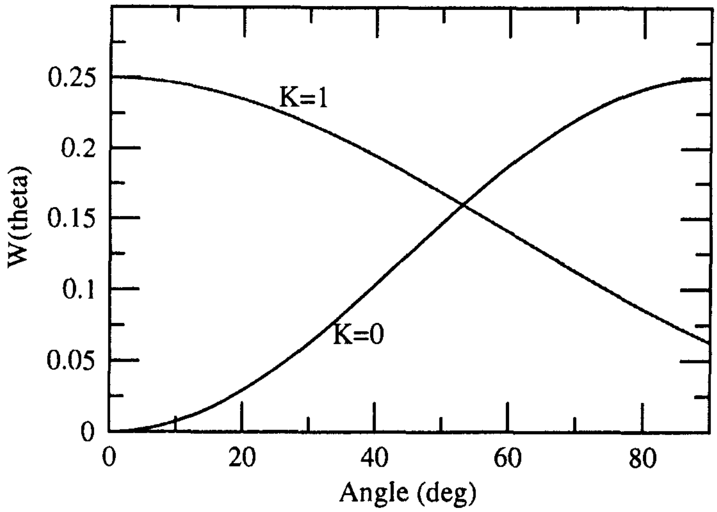

Figure 2.14: Fragment angular distribution for gamma induced fission of even-even nucleus calculated using equations (K=0) and (K=1).

transition state with $K = 1$. Giving equal weight to all the combinations of K and M gives

$$W^{J=1}_{M=\pm1,K=\pm1}(\theta) = \frac{3}{2}\left\{\frac{|D^1_{1,1}(\theta)|^2}{4} + \frac{|D^1_{-1,1}(\theta)|^2}{4} + \frac{|D^1_{1,-1}(\theta)|^2}{4} + \frac{|D^1_{-1,-1}(\theta)|^2}{4}\right\} \tag{2.39}$$

The angular distribution calculated for different values of K are in figure 2.14. Dipole fission of an even-even nucleus may occur through either $K = 0$, $K = 1$ or some combination of these two levels. For $K = 0$ transition, the fragment distribution peaks in a direction perpendicular to the incident gamma ray and goes to zero in direction parallel to the beam. For $K = 1$, the peak is at zero degree and it reduces by a factor of two at 90 degree. The angular distribution for gamma induced fission in ^{232}Th and ^{234}U is shown figure 2.15. It can be seen from the distribution that is peaking at 90^0 that the contribution is mainly from dipole fission with $K = 0$. At higher energies, contribution from higher values of J also will come into the picture.

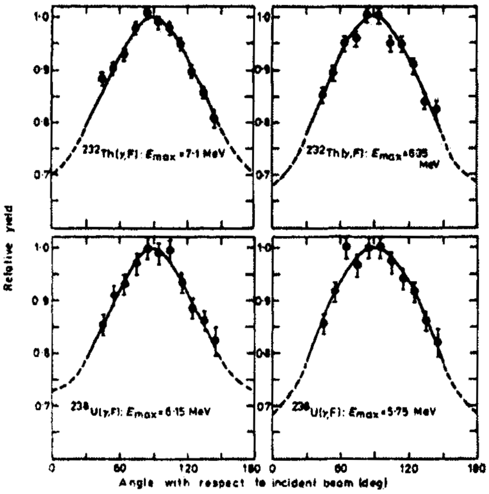

Figure 2.15: Measured angular distributions for ^{232}Th and ^{238}U at different energies.[Nair 1977]

2.6.3.2 Statistical Saddle Point Model, SSPM

The fission fragment angular distribution for a saddle-point nucleus with specific quantum numbers was described in the previous section. This theory can be extended to higher excitation energies where the transition levels can be described by statistical methods [Halpern 1957] , as explained below.

The density of levels in the transition nucleus with spin J and its projection K along the nuclear symmetry axis is given by the approximate relation

$$\rho(J,K) \propto \exp\left(\frac{E - E_{rot}^{J,K}}{t}\right) \tag{2.40}$$

where E is the total energy and $E_{rot}^{J,K}$ is the rotational energy of the transition state (J,K) and t is the thermodynamic temperature, which is assumed to be constant for small changes of excitation energy. The thermodynamic energy available to the nucleus is $E - E_{rot}^{J,K}$. The rotational energy of the nucleus at the saddle-point deformation is

$$E_{rot}^{J,K} = \frac{\hbar^2}{2I_{\perp}}(J^2 - K^2) + \frac{\hbar^2}{2I_{\parallel}}K^2 \tag{2.41}$$

where $I_\perp$ and $I_\parallel$ are the nuclear moments of inertia about the axes perpendicular and parallel to the symmetry axis, respectively. Substituting equation 2.41 into 2.40 gives

$$\rho(J,K) \propto \exp\left(\frac{E}{t} - \frac{\hbar^2 J^2}{2I_\perp t} - \frac{\hbar^2 K^2}{2t}\left[\frac{1}{I_\parallel} - \frac{1}{I_\perp}\right]\right) \tag{2.42}$$

For a particular value of J the K distribution becomes

$$\rho(K) \propto \exp\left\{\frac{\hbar^2 K^2}{2t}\left[\frac{1}{I_\parallel} - \frac{1}{I_\perp}\right]\right\} \tag{2.43}$$

This is equivalent to a Gaussian K distribution

$$\rho(K) \propto \exp\left(\frac{K^2}{2K_0^2}\right) \; for\, K \leqslant J \tag{2.44}$$

where the width of the K distribution $K_0^2 = tI_{eff}/\hbar^2$. The effective moment of inertia $\frac{1}{I_{eff}} = \frac{1}{I_\parallel} - \frac{1}{I_\perp}$. The nuclear temperature t can be calculated using the expression

$$t = \sqrt{\frac{E + Q - B_f(J) - B_{rot} - E_n}{a}} \tag{2.45}$$

where E is the energy brought in by the projectile, Q is the binding energy released/consumed in the fusion process, B_f is the fission barrier, E_n is the energy carried away by the pre-scission neutrons, B_{rot} is the energy expended on rotation and a is the level density parameter. If t and K_0^2 are known, the moment of inertia of the saddle point nucleus can be calculated and this gives information about the shape of the saddle point nucleus.

The angular distribution for a particular J is given by the expression

$$W^J(\theta) = \sum_{K=-J}^{J} \frac{(2J+1)\left|D^J_{M,K}(\theta)\right|^2 \exp\left(\frac{-K^2}{2K_0^2}\right)}{\sum_{K=-J}^{J} \exp\left(\frac{-K^2}{2K_0^2}\right)} \tag{2.46}$$

The total angular distribution can be obtained by summing over all the J values. The total angular momentum is obtained by adding up the orbital angular momentum L , target spin I_0 and the projectile spin s. Defining the channel spin $S = I_0 + s$, the exact equation for the angular distribution is

$$W(\theta)=\sum_{J=0}^{\infty}\sum_{M=-S}^{M=+S}\left\{\sum_{\ell=0}^{\infty}\sum_{S=|I_0-s|}^{I_0+s}\sum_{\mu=-I_0}^{+I_0}\frac{(2J+1)T_\ell\left|C_{M,0,M}^{S,\ell,J}(\theta)\right|^2\left|C_{\mu,M,-\mu,M}^{I_0,s,S}(\theta)\right|^2}{\sum_{\ell=0}^{\infty}(2\ell+1)T_\ell}\right\}\times W^J(\theta) \tag{2.47}$$

where T_ℓ is the transmission coefficient of the ℓ^{th} partial wave. $C_{M,0,M}^{S,\ell,J}$ and $C_{\mu,M,-\mu,M}^{I_0,s,S}$ are the Clebch-Gordan coefficients. If we ignore the target and projectile ground state spins equation 2.47 can be simplified to give

$$W(\theta)=\sum_{J=0}^{\infty}(2J+1)T_J\sum_{K=-J}^{J}\frac{(2J+1)\left|D_{M,K}^{J}(\theta)\right|^2\exp\left(\frac{-K^2}{2K_0^2}\right)}{\sum_{K=-J}^{J}\exp\left(\frac{-K^2}{2K_0^2}\right)}. \tag{2.48}$$

The angular distribution of fission fragments depends on two factors: the angular momentum brought in by the projectile and the fraction of it being converted into the orbital angular momentum of the compound nucleus. This latter fraction is characterized through the parameter K, the projection of angular momentum along the symmetry axis. It has been shown earlier that K can be related to the fission fragment angular distribution under the assumptions: (a) value of K does not change from saddle to scission, which means that the Coriolis forces acting on the system as it elongates from saddle to scission are not strong enough to alter the K value selected at the saddle point. (b) Fission fragments are emitted along the nuclear symmetry axis at saddle point. The angular momentum distribution may be controlled by choosing the projectile and its energy. However, K distribution is decided by the nucleus itself and it can be deduced from the measured angular distribution. The angular distributions are controlled by fluctuations in the orientation of the fission decay axis with respect to the total angular momentum vector. K_0^2 is a measure of this fluctuations and a larger value makes the distribution more isotropic.

The anisotropy of fragment angular distribution is defined as ratio of emissions in the directions parallel and perpendicular to the beam direction

$$A = W(180)/W(90) \tag{2.49}$$

and can be calculated from equation 2.47. However, at low anisotropy values one can use the approximate expression

$$A = 1 + \frac{\langle J^2 \rangle}{K_0^2} \tag{2.50}$$

where $\langle J^2 \rangle$ is the second moment of the compound nucleus spin distribution, which can be extracted from the fusion excitation function. It can be seen from equation 2.50 that a larger value of K_0^2 , width of K distribution, results in a more isotropic distribution. Compound nucleus close to spherical shape are easier to tilt and will have large K_0^2 and hence a more isotropic fragment distribution. The Statistical Saddle Point Model, SSPM, provides a relation between the nuclear temperature, the nuclear shape and the distribution of K values at saddle point. Thus, information about the shape of the saddle point nucleus can be extracted from the measured fragment angular distributions.

Fission fragment angular distributions have been studied for a variety of projectiles including neutrons, protons, alphas and heavy ions for different excitation energies. Some of the important experimental observations are:

- The fragments have the largest differential cross section in the directions forward and backward along the beam.
- The anisotropies are larger for heavier projectiles and smallest for neutrons and protons.
- The anisotropy shows an increase when the excitation energy is sufficient for fission after neutron evaporation.
- The anisotropy decreases as the Z^2/A value of the target increases.

The preference along the beam direction can be qualitatively explained for a system having zero target and projectile spins. In this case, compound nucleus angular momentum distribution is due to the different impact parameters of collision. The compound nucleus angular momentum vectors will be uniformly distributed in a direction perpendicular to the beam direction. The rotating nuclei splits along the symmetry axis and an isotropic distribution will result if all K values are equally probable. But the compound nucleus is elongated and for a particular value of J the rotational energy is minimum for a rotation perpendicular to the symmetry axis ($K = 0$) since $I_{\perp}$ is larger than $I_{\parallel}$. This will make the density of levels more for states with $K = 0$, more favorable Boltzmann factor according to the equation 2.40. Fragments from levels with $K = 0$ will be aligned parallel and levels with $K = J$ will be aligned perpendicular to the beam. Integration over all the directions will lead to a concentration of fragments in the beam direction.

The degree of anisotropy depends on both J and K distributions. Increasing the projectile energy or mass will increase the weighting of high J states in the J distribution and increase the anisotropy. The K distribution is an internal property of the compound nucleus. But increasing the excitation energy increases the temperature and hence the value of K_0^2. Hence the excitation energy dependence of anisotropy is decided by the effect of energy on the J and K distributions. Anisotropy increases with the projectile mass due to the larger angular momentum brought in.

While interpreting the experimental results using SSPM, the basic assumptions made by the theory must be kept in mind. SSPM assumes the formation of a fully equilibrated compound nucleus, without retaining any memory of the entrance channel configuration. The compound nucleus is assumed to be formed by trapping the incoming nuclei inside the pocket of the potential energy curve. At high angular momentum values the height of the barrier becomes comparable to the nuclear temperature and the conditions for the formation of the fully equilibrated compound nucleus is violated. For deformed targets, the projectile can come in contact with the tip of the target, feeling less repulsion due to the larger separation from the center of the average Coulomb potential. The compound system formed that way also may undergo fission without forming a fully equilibrated compound nucleus. Any system which undergoes fission before equilibrating fully can be said to

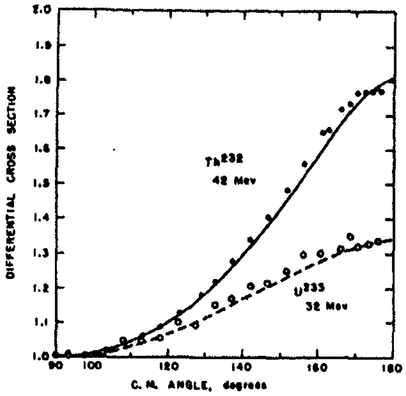

Figure 2.16: Fragment angular distribution for light ions.

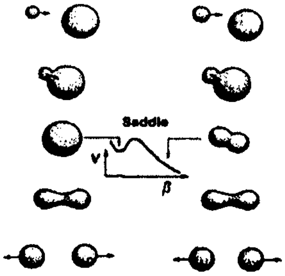

Figure 2.17: Schematic of fusion-fission modes. Fission after forming a compound nucleus relaxed in all degrees of freedom is shown on the left. In the other case a dinucleus is formed and it undergoes fission before forming a fully equilibrated compound nucleus.

retain the memory of the entrance channel parameters.

Early experimental results using nucleons and alpha particles were explained well using SSPM. For example, measured angular distributions along with SSPM calculated results for alpha induced fission of ^{233}U and ^{232}Th [Vandenbosch 1961] are shown in figure 2.16. These results gave credibility to the concept of a compound nucleus formed by fusion of the target-projectile system and its subsequent decay through fission and evaporation channels. The near isotropic angular distribution of fragments suggested that compound nucleus undergoes several rotations before fissioning and fission time scales were estimated from the number of pre-scission neutrons emitted.

2.6.3.3 Deviations from SSPM

The advent of higher energy heavy ion accelerators during the eighties enabled the study of fusion-fission in heavy systems involving large values of angular momenta. The measured anisotropy values showed deviations from the SSPM predictions at all projectile energies for:

- Compound nucleus with large angular momentum values
- Heavy projectiles resulting in lesser mass asymmetry
- Systems with large charge product values

These deviations from SSPM predictions are mostly attributed to the violation of the basic assumption namely, formation of a fully equilibrated compound nucleus on which the theory is founded, rather than the failure of the theory. It is suggested that in many heavy-ion-induced fission reactions showing anomalous anisotropy values, the observed fission events may be an admixture of compound nucleus (CN) and non-compound nucleus (NCN) fission events. The two different modes are shown schematically in figure 2.17. Fast fission [Lebrun 1979], quasi-fission [Back 1985] and pre-equilibrium fission [Ramamurthy 1985] are the NCN fission modes proposed by different groups for explaining the above observations.

Fast fission (FF) is expected when the height of the fission barrier, which is a function of angular momentum, becomes comparable to the nuclear temperature. This happens for high projectile energies and targets with high fissility values. The quasi-fission (QF) takes place when the unconditional saddle point shape is more compact than the entrance channel contact configuration. This happens due to high Coulomb repulsion and is expected for product of charges $Z_1Z_2 > 1600$. The pre-equilibrium fission (PEF) events describes the NCN events occurring on a time scale comparable to the relaxation time of the K-degrees of freedom when the fission barrier of the composite system becomes comparable to its temperature. The K distributions of PEF will be the product of the entrance channel K distribution and the saddle point K distribution, and the narrower of the above decides the

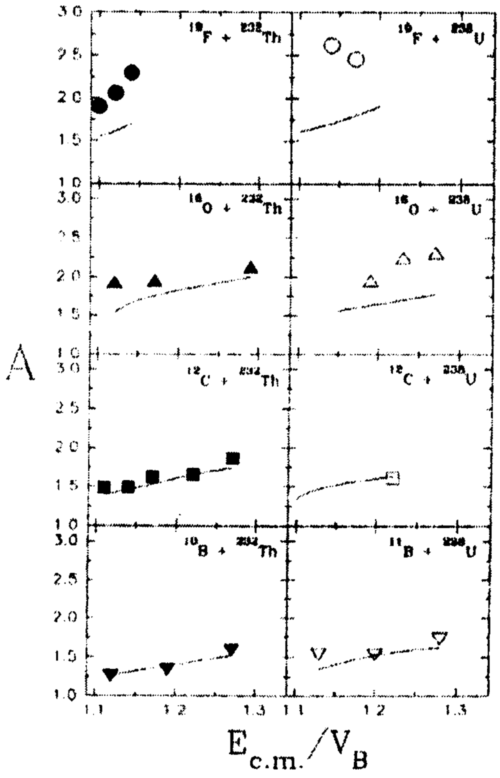

Figure 2.18: Anisotropy for systems with different entrance channel mass asymmetry values.[Kailas 1997]

fragment anisotropy. PEF events are expected even when the conditions for FF and QF are not satisfied. According to the PEF model, the probability of NCN events depends on the value of entrance channel mass asymmetry α with respect to the Businaro-Gallone [Businaro 1955] critical mass asymmetry. Systems entering with $\alpha > \alpha_{BG}$ proceeds towards a mononuclear shape resulting in a CN event, and cases with $\alpha < \alpha_{BG}$ relaxes towards a mass symmetric dinuclear shape and ends in NCN fission. Measured anisotropies along with SSPM predictions for several systems with different entrance channel mass asymmetries are shown in figure 2.18.

2.6.3.4 Anomalous anisotropy with deformed targets

Another interesting phenomena is the observed anomalous anisotropy at near barrier energies for targets having a non-spherical ground state shape [Murakami 1986]. This increase in anisotropy near the barrier has been attributed to orientation dependent quasi-fission by Hinde [Hinde 1996] but the results reported by Majumdar [Majumdar and Biswas 1996] contradicts this argument. The PEF model explains the anomalous anisotropy of deformed target by the shifting of the value of α_{BG} due to channel coupling effects.

However, for targets having large ground state spins, the departure from SSPM is less drastic [Lestone 1997]. The presence of either target or projectile spin seems to reduce the abnormal increase in anisotropy values at near-barrier energies. [Lestone 1997, Nayak 2000]

2.6.4 Objectives of the present study

In the present study, we have decided to investigate mainly two systems ^{13}C+^{232}Th and ^{13}C+^{235}U starting from sub-barrier energies to well above barrier. Investigations in the past [Ramamurthy 1990, Mein 1997] have shown that ^{12}C+^{232}Th ($\alpha > \alpha_{BG}$)followed the SSPM predictions above Coulomb barrier. In a recent study Behera et.al. [Behera 2001] have reported anomalous anisotropies for ^{14}N+^{232}Th ($\alpha > \alpha_{BG}$) over the entire energy range spanning the barrier. We have decided to investigate ^{13}C+^{232}Th, whose mass asymmetry lies in between the above two systems, for energies covering the barrier.

If the above barrier results are in agreement with SSPM, we can conclude that the $^{13}C+^{232}Th$ reaction proceeds through the formation of a fully equilibrated compound nucleus. The results near barrier can be compared with that of $^{12}C+^{232}Th$ reaction to investigate the effect of the non-zero spin of the projectile on the nature of anisotropy near and below barrier energies.

Another system we are investigating is $^{13}C+^{235}U$ leading to the compound nucleus ^{248}Cf . The same compound nucleus, formed by different entrance channels like $^{11}B+^{237}Np$, $^{12}C+^{236}U$ and $^{16}O+^{232}Th$, has been studied earlier [Kailas 1999]at above barrier energies. The present study will look for the dependency of anisotropy on the entrance channel. It has been reported [Lestone 1997] that the anomalous increase in anisotropy near the barrier is related to the ground state spin of the target. We have studied the $^{13}C+^{235}U$ system where the target spin is 7/2. The results of the zero spin ^{232}Th and the non-zero spin^{235}U targets using the same projectile can be compared to investigate this aspect.

Bibliography

[Back 1985]	Back B B et al, Phy. Rev. C Vol. 32(1985)
[Balantekin 1998]	Balantekin A B et al., Rev. of Modern Physics Vol.70 (1998)
[Balantekin 1983]	Balantekin A B et al, Phy. Rev C Vol. 28(1983)
[Beckerman 1981]	Beckerman et al. Phy. Rev C Vol.23 (1981)
[Beckerman 1983]	Beckerman Phy. Rev. C Vol. 28(1983)
[Beckerman 1988]	Beckerman M, Rep. Prog. Phy. 51(1988)
[Behera 2001]	Behera B R et al, Phy. Rev. C64 (2001)
[Behkami 1968]	Behkami et al, Phy. Rev. Vol. 171(1968)
[Bjornholm 1980]	Bjornholm S et al, Rev. Mod. Phy. Vol 52(1980)
[Bohr 1939]	Niels Bohr, Phy. Rev. Vol 56(1939)
[Britt 1971]	Britt H C et al, Phy. Rev. C Vol. 4 (1971)
[Businaro 1955]	Businaro U L et al, IL Nuovo Cimento, Vol. I.N.4 (1955)
[Cramer 1970]	Cramer J D et al, Phy. Rev. C Vol. 2 (1970)
[Dasgupta 1998]	Dasgupta M et al, Annu. Rev. Nucl. Part. Sci. (1998)401-61

[Dasso 1983]	Dasso C H, S. Landowne and A. Winther, Nucl. Phys. A407, 221 (1983)
[Flynn 1972]	Flynn K F et al, Phy. Rev. C Vol. 5 (1972)
[Flynn 1975]	Flynn K F et al, Phy. Rev. C Vol. 12 (1975)
[Frankel 1947]	Frankel S, Metropolis N, Phy. Rev. Vol. 72 (1947)
[Halpern 1957]	Halpern I and Strutinsky V M, Proc. of Second United Nations International Conference on the Peaceful Uses of Atomic Energy, Geneva (1957)
[Hahn 1939]	Hahn O and Strassman F, Naturwissenschaft 27 (1939) 11
[Hill, Wheeler 1953]	Hill D L & Wheeler J A, Phy. Rev. vol 89(1953)
[Hinde 1996]	Hinde D J et al, Phy. Rev. C Vol. 53(1996)
[Kailas 1997]	Kailas S, Phy. Rep. 284 (1997)
[Kailas 1997]	Kailas S, J. Phy. G: Nucl. Part. Phy. 23 (1997)
[Kailas 1999]	Kailas S et al, Phy. Rev. C Vol. 59(1999)
[Krappe 1979]	Krappe H J et al, Phy. Rev. C Vol. 20(1979)
[Lebrun 1979]	Lebrun C et al, Nuc. Phy. A 321(1979)
[Leigh 1993]	Leigh J R et al, Phy Rev C Vol 47(1993)
[Lestone 1997]	Lestone J P et al, Phy. Rev. C56(1997)
[Majumdar and Biswas 1996]	Majumdar N, Biswas D C et al, Phy. Rev. C 53(1996)

[Mayer 1948]	Mayer M G, Phy. Rev. Vol 78 (1950)
[Mayer 1950]	Mayer M G, Phy. Rev. Vol 78 (1950)
[Mein 1997]	Mein J C et al, Phy. Rev. C Vol. 55 (1997)
[Moller 2001]	Moller P et al, Nature Vol. 409 (2001)
[Murakami 1986]	Murakami T et al, Phy. Rev. C Vol 34(1986)
[Nair 1977]	Nair S et al, J. Phys. G Nuc. Phy. Vol. 3 (1977)
[Ramamurthy 1985]	Ramamurthy V S et al, Phy. Rev. Lett. 54(1985)
[Ramamurthy 1990]	Ramamurthy V S et al, Phy. Rev. Lett. 65,25(1990)
[L.I.Schiff]	Schiff L I, Quantum Mechanics, McGraw Hill Book Co.
[Strutinsky 1967]	Strutinsky V M, Nuc. Phy. A95(1967) p420-442
[Thomas 2003]	Thomas R G et al, Phy. Rev. C 67 (2003)
[Vandenbosch 1961]	Vandenbosch R et al, Phy. Rev. Vol. 124 (1961)
[Wong 1973]	Wong C Y, Phy. Rev. Lett. Vol. 31(1973)

Investigation of Fusion Reactions of Heavy Ions And Development of Necessary Instrumentation

A Thesis submitted to the University of Calicut
for the partial fulfillment of the requirements
for the degree of
Doctor of Philosophy in Physics

Ajith Kumar B.P.

Department of Physics
University of Calicut
May, 2007

Chapter 3

Experimental Setup

The objective of the experiment is to measure the differential fission cross section $d\sigma/d\Omega$ for the ^{235}U and ^{232}Th target nuclei using ^{13}C beam. The fission detectors should be capable of separating the fission fragments from the ejectiles resulting from other processes like quasi-elastic scattering. The fission yield is measured by placing the detectors at different angles with respect to the beam direction. Since the amount of incident beam during each measurement could be different, the fission yield is normalized using the amount of Rutherford scattered beam into a monitor detector kept at a fixed angle. The process is repeated at beam energies starting from below the Coulomb barrier to energies well above the barrier.

A schematic of the experimental setup, that is common to the study of both the systems, is shown in figure 3.1. In this chapter we describe the ion beam, the target, detectors, electronics used for signal processing and the data acquisition system used for studying the ^{235}U and ^{232}Th target nuclei using ^{13}C beam. Minor differences are described in the coming chapters explaining the respective reactions.

3.1 The Beam

For doing heavy ion fusion experiments in the laboratory, we require high speed projectiles that can overcome the Coulomb repulsion with the target

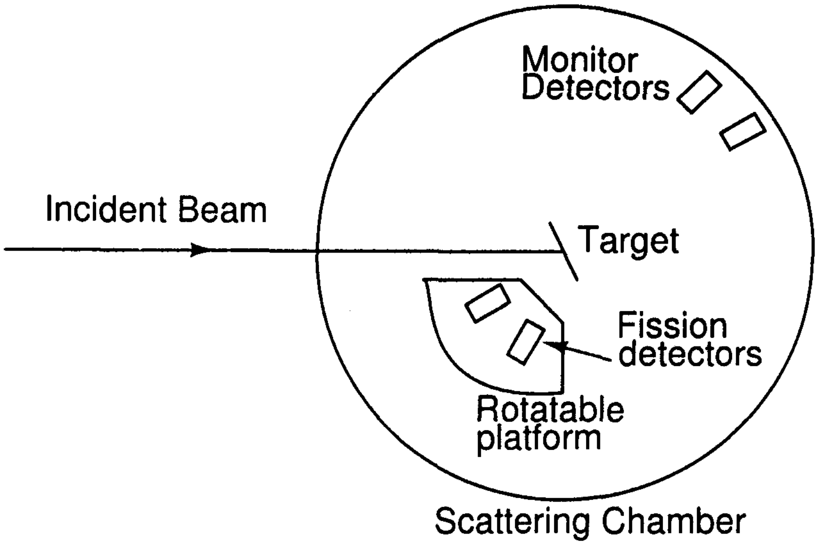

Figure 3.1: Schematic of the experimental setup for measuring the angular distribution of fission fragments.

nucleus, which is provided by a particle accelerator. There are several kinds of accelerators that uses DC or radio frequency fields to accelerate charged ions. Van de Graff type machines use a DC potential to accelerate ions. and a Tandem accelerator is a modified version of it. The high voltage terminal is kept inside a pressure vessel filled with some gas having high dielectric constant. In a tandem accelerator, the negatively charged ion gains energy by attraction to the very high positive voltage at the geometric centre of the pressure vessel. When it arrives at the high voltage terminal, some electrons are stripped from the ion. The ion then becomes positive and accelerated away by the high positive voltage. Thus, this type of accelerator is called a 'tandem' accelerator. The accelerator has two stages of acceleration, first pulling and then pushing the charged particles. The output energy is given by the relation $E = q(V + 1)$, where V is the terminal potential and q is the charge state of the positive ion. The most probable charge state for a given ion is a function of the terminal potential

Present study of fusion-fission was done using ^{13}C beam from the Tandem Van de Graaff Accelerators at IUAC, New Delhi and the BARC-TIFR, Mumbai. We have varied the terminal potential from 10 to 12 Million Volts to produce ^{13}C ions ranging from 60 MeV to 84 MeV. Being DC machine the Van de Graaff accelerators give very good energy resolution and steady beam currents.

3.2 The Targets

The nuclear reaction happens when the high energy projectile hits the target. There are several considerations for preparing suitable targets. The target material thickness is generally in several hundred $\mu gm/cm^2$. A thick target will have energy degradation inside the target and the measurement of the energy dependency of the reaction becomes less accurate. On the other hand a very thin target results in low yield and will require longer time to complete the experiment. Some of the target material can be made as self supporting. If that is not possible, the target material is deposited on some backing material like aluminium. The atomic numbers of the target and backing material should not far apart to avoid any contamination in the reaction products detected.

To study the ^{13}C+^{232}Th system, a 1.8 mg/cm^2 thick thorium foil is used as the target. The target is self supporting and mounted on a frame. For the ^{13}C+^{235}U system, the uranium target was made by depositing 200 to 300 μgm/cm^2 thick ^{235}U isotope on an aluminium backing. The uranium deposited side was kept towards the beam to avoid any energy degradation due to the aluminium backing. The scattered particles reaching the monitor detector will pass through the aluminium but their energy measurement is not important in our experiment.

3.3 The Charged Particle Detectors

Charged particles are detected by their interaction with matter [Knoll 1978]. When a charged particle enter a material media it interacts with the atoms of the media along its track loosing kinetic energy. The velocity decreases gradually and if the thickness of the material is sufficient it comes to a complete halt. The specific energy loss of a charged particle inside a material is given by relation known as the Bethe formula expressed as

$$-\frac{dE}{dx} = \frac{4\pi e^4 z^2}{m_0 v^2} NZ \left[\ln \frac{2m_0 v^2}{I} - \ln\left(1 - \frac{v^2}{c^2}\right) - \frac{v^2}{c^2} \right] \tag{3.1}$$

where v and ze are the velocity and charge of the primary particle, N and Z are the number density and atomic number of the material, m_0 is the electron rest mass and I is the average ionization potential. For non-relativistic particles only the first term inside the bracket of equation 3.1 is significant. From the expression 3.1, it can be seen that the specific energy loss is proportional to the square of the charge of the incident particle and inversely proportional to its mass. The $1/v^2$ dependency implies that the dE/dx is inversely proportional to the energy.

The specific energy loss along the track is given by the Bragg curve . For light charged particles like protons and alpha particles the specific energy loss is maximum towards the end, due to the decreasing particle velocity. However for fission fragments the specific energy loss decreases along the track. Since they enters with a very large positive charge, the electron pickup starts from the very beginning. The decrease in dE/dx due to the reduction in charge is more dominant than its increase due to the reduction in velocity.

When a charged particle enters the detector volume they ionize the neutral atoms inside the detector which results in the creation of electric charge pairs. Electron-ion pairs are created in gas detectors and electron-hole pairs in solid state detectors. An electric field is applied across the detector to collect this charge and generate an electrical signal. The time required to collect the charge depends on the properties of the detector and the electronic circuits used. The amount of charge collected is proportional to the number of charge pairs created and hence to the energy deposited by the incident particle. The electrical pulse output from the detector contains information about the properties of the incident particle like its kinetic energy, time of arrival etc. Detectors have been developed using gas, liquid and solid media each having its own characteristics. Detector medium having low ionization energy generates more number of charge pairs and gives better resolution. Higher density materials gives better stopping power and results in smaller detector volume. Due to these reasons, solid state detectors using semiconductor materials like silicon, germanium etc. have become very popular.

3.3.1 Semiconductor Detectors

In principle a block of semiconductor material with two *ohmic* contacts on two opposite ends for charge collection should act as a radiation detector. However, we need to consider the effect of the voltage need to be applied across the active volume of the detector to collect the charges. Due to the finite resistivity of the available semiconductor materials, except for high purity germanium, this results in unacceptable levels of leakage current. The method to overcome this is to configure the detector as a PN junction and use it in the reverse biased mode. Diffused Junction Detectors, Surface Barrier Detectors and Passivated Planar detectors are commonly used junction diode detectors.

The Diffused Junction Detectors are fabricated by starting with a homogeneous crystal of p-type material and diffusing n-type impurity to one surface to form a PN junction. The thickness of the n-type layer formed is generally up to 2 microns. Since the n-type surface layer is heavily doped compared to the p-type crystal, the depletion region primarily extends into the p-type region. Much of the surface layer remains outside the depletion region and act as a dead layer where the particle looses energy before entering the detector volume. Surface Barrier Detectors are made by creating electron traps on one surface of a p-type crystal, which acts like a PN junction. They are fabricated by etching the surface and evaporating a thin layer of gold on it. The thickness of the dead layer in an SBD could be reduced to several tens of nanometers.

3.3.2 Particle identification by E-ΔE telescope

The dependency of specific energy loss on mass and energy can be utilized for particle identification. In a E-ΔE telescope, two detectors are placed one

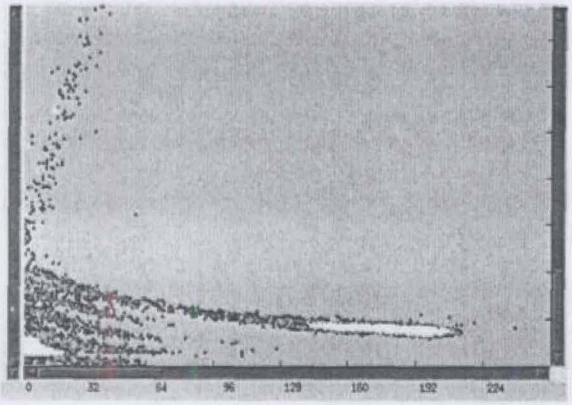

Figure 3.2: An E-ΔE plot of ^{13}C+^{235}U reaction products. Total energy E+ΔE is along x-axis and ΔE is along y-axis. A gas ionization chamber is used as ΔE detector and a Silicon Surface Barrier detector for E.

after the other. The particle deposits a fraction of its energy in the first detector, called the ΔE detector, and the remaining energy in the E detector. From equation 3.1 it can be seen that the energy loss in the ΔE detector is proportional to z^2/v^2 and the total energy loss is proportional to mv^2, multiplying them gives z^2m. A plot of ΔE vs E+ΔE will form different hyperbolas grouping particles having same values of z^2m. It is very important that the dead layer should be very small if a solid state detector is to be used as a ΔE. In the case of gas ΔE detectors the fraction of energy deposited in it can be controlled by varying the effective thickness by adjusting the gas pressure.

Figure 3.2 shows the^{13}C+^{235}U reaction products captured by an E-ΔE detector. The hyperbolas representing quasi-elastic scattered particles having different z^2m values are clearly visible on the lower side. The upper portion shows the fission fragments which deposited most of the energy in the ΔE detector. We have used this method to separate fission fragments from other reaction products.

3.3.3 Measuring Fission Fragment Angular Distribution

E-ΔE telescopes described in the previous section were used for identifying the fission fragments. Initially we used gas detectors and later switched over to thin Silicon Surface Barrier detectors when they became available. Two telescopes were mounted on a rotating platform at an angular separation of 20^0. The platform is rotated to take measurements from 170^0 to 80^0 at every 10^0 intervals. The telescopes have a collimator of 4 to 5 mm diameter and kept at a distance of around 13cm from the target. A larger collimator can improve the count rates but may add to the error in the determination of the angle.

The ΔE detectors have thicknesses between 10 to 20 microns and the E detectors behind are 300 microns thick. The fission fragments get stopped in the ΔE detector while the scattered particles deposit very little energy in the ΔE detector. Due to this reason it is possible to separate the fission fragments from the light particles resulting from non-fission reactions using the thin detector itself. The number of fission fragments are extracted from a 2D plot of the energy deposited in E and ΔE detectors.

Two monitor detectors are placed at fixed forward angles to measure the elastic scattering. One monitor detector is required for normalization of the fission counts measured at different angles and also to calculate the absolute fission cross section, using the theoretical value of Rutherford scattering cross section and the second one is kept for cross checking. The distance from the target and the aperture of the monitor detectors are chosen to record comparable count rates on fission and monitor detectors.

3.4 Signal Processing

Figure 3.3 shows a rough schematic of a detector. The charge pairs created inside the detector by the incoming particle results in a voltage pulse across the RC network connected to the detector. The rise-time of this pulse depends on the time required for collecting the charge and the fall time depends on the charge collection circuit. The amount of charge depends on the energy

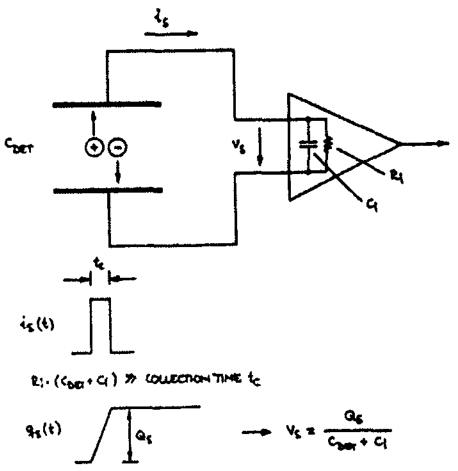

Figure 3.3: Rough schematic of a detector and the charge collection circuit.

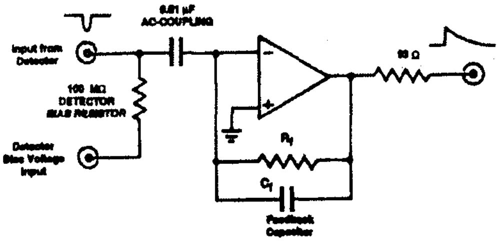

Figure 3.4: Simplified schematic of a charge sensitive ac coupled pre-amplifier

of the particle and on the detector properties. The amount of charge is very small and it need to be processed by a pre-amplifier and a shaping amplifier before getting digitized.

3.4.1 The Pre-amplifier

The primary function of the pre-amplifier is to extract the signal from the detector without degrading the signal to noise ratio. There are several types of pre-amplifiers like the current sensitive, charge sensitive and parasitic capacitance pre-amplifier. For energy spectroscopy applications mostly charge sensitive pre-amplifiers are used. A schematic of a charge sensitive pre-amplifier is shown in figure 3.4. The signal from a semiconductor detector or an ionization chamber is a current pulse lasting for few nanoseconds to several hundred nanoseconds depending on the type and size of the detector. The charge sensitive pre-amplifier output is proportional to the quantity of charge inside the current pulse. Since it integrates charge on the feedback capacitor, its gain is not sensitive to the changes in detector capacitance. The output pulse from the pre-amplifier has a small rise-time and long fall-time as shown in the figure 3.5 .This is further processed by using a shaping amplifier to get the energy information. The pre-amplifier also provides a timing signal output, that in our case is used for triggering the data acquisition system.

3.4.2 The Shaping Amplifier

In order to ensure complete charge collection, the pre-amplifiers are generally adjusted to have a long decay time for the output pulse. When the particle arrival rates are high this will result in overlapping. The solution to this is to shape the pulse to have a fixed duration. The amplitude need to be preserved since it contains the information about the amount of charge collected. Pulse shaping is generally done by a differentiation followed by several integrations using RC networks. The differentiation eliminates the long tail, the low frequency component, and the integrations eliminates the sharp rising edge. The CR-RC pulse shaping will result in a Gaussian shaped pulse whose amplitude is proportional to the charge collected and hence to the energy of the incident particle. This pulse height is digitized to generate the energy spectrum of the incident particles.

3.4.3 The Timing Filter Amplifier and Discriminator

When the timing signal from the pre-amplifier is of sufficient amplitude it can be directly fed to a discriminator. The timing signal from a charge sensitive pre-amplifier need to be amplified before giving to a discriminator. Wide-band Timing amplifiers or Timing Filter Amplifiers generally are used for this purpose. The output of the TFAs are given to a Constant Fraction

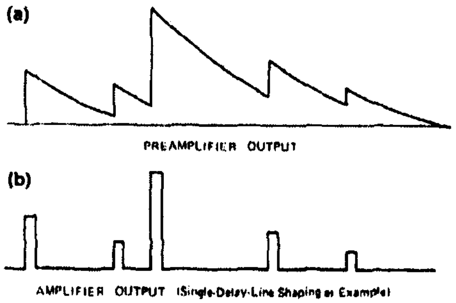

Figure 3.5: (a) Output of the pre-amplifier. (b) After shaping, to remove the long tails. Shown an ideal case. Actual output of the CR-RC shaping circuit will be Gaussian.

Discriminator to generate the logic level signals required for the logic circuits doing the event detection.

3.5 The Data Acquisition System

From the signals generated by the detectors the events of interest are selected based on the reaction one is interested in. For the selected events all of the detector signals are digitized and stored as a group. This is usually referred as the event mode data acquisition. An event mode data packet will have recorded data from a group of detectors generated by a particular event or reaction. The signal generated by the logic selecting the events of interest is called the event trigger. In addition to event mode or co-related data we need to collect data from individual detectors whenever they generate a signal. This is the Singles Data which comes from independent detectors. Most of the time the processing done for these signals are to generate a histogram and record the total count received during a particular interval, for normalization purposes. The system also should have options to read and record scalars etc., which collects information about the number of particles recorded by certain detectors.

3.5.1 Freedom, The Data Acquisition at IUAC

Freedom [Ajith 2005] is a Data Acquisition System developed at IUAC, New Delhi, to acquire and analyze data from the Accelerator based experiments. A hardware schematic of the DAS is shown in figure 3.6. The NIM and CAMAC hadware standards are followed to implement the system. A Hardware schematic of the system is shown in figure 3.6 .

The new Data Acquisition System has been designed to support the various experimental facilities associated with the NSC Tandem Accelerator, like the Gamma Detector Array & the Heavy Ion Reaction Analyzer . The system is capable of running on a single computer or on a network, under LINUX operating system. Implementation of this project is entirely using Free Software tools. The objective is to collect experimental data, save them to some storage media and to perform on-line analysis. Experimental signal conversion is performed by various NIM & CAMAC modules and data is read through CAMAC dataway. Events of experimental interest are detected by hard-wired logic and the system is triggered to record them. For achieving higher acquisition speeds intermediate buffering of data is performed. A List Processor module, Hytec LP 1340, is used for collecting and buffering the Event Mode data. The LP in tandem with a specially designed Trigger Generator module performs the first phase of reading data. Data from LP module is then transferred to a ring buffer in the computer memory by using 16 bit DMA transfer. The data is send for on-line analysis and display over a TCP/IP network and also saved to a high capacity hard-disk, and then to cartridge tapes. Singles mode data is taken by Canberra 8075 ADCs interfaced to home-made CAMAC histogram generator modules. The user interface is implemented using X-window graphics. The fully menu driven interface allows the configuration of the CAMAC hardware, generating one dimensional and two dimensional spectra, mathematical operations on data, gating etc.

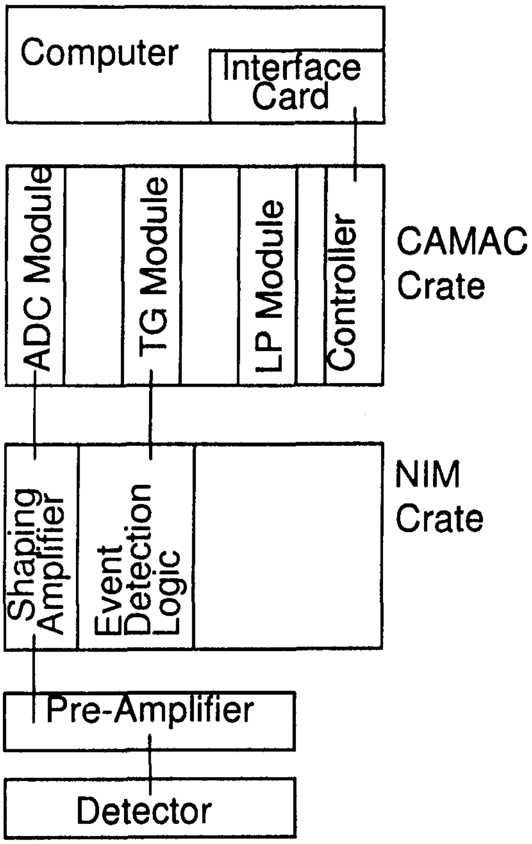

Figure 3.6: Hardware Schematic of the 'Freedom' Data Acquisition System. There is a Pre-Amplifier, Shaping Amplifier and Analog to Digital Converter channel for each signal from the Detectors connected to the system. Only a single channel is shown in the figure but 'Freedom' can support upto 50 detector signals. The Pre-amplifiers are generally kept closer to the Detector. The Shaping amplifier and other analog signal processing modules are located inside NIM Crates. The Digitization of signals and local storage of data are done using CAMAC modules.

3.5.1.1 The Hardware

The hardware consists of a CAMAC branch highway using KSC3922 Crate controllers interfaced to a PC, called the server computer, with KSC2927 interface card. A LIST PROCESSOR module, Hytec LP1340 which is capable of executing a set of pre-programmed CAMAC commands when triggered, is located in one of the crates. A simplified hardware schematic is shown in figure 3.6. The ADCs, TDCs etc. collecting the event mode data are also located in the same Crate so that LP can access them. There can be upto seven Crates on the highway and the modules like scalers, histogram generators etc. can be plugged in any of them. Fast signals from the detectors used in the experimental setup is processed by hard-wired logic to generate a Master Trigger indicating an event of experimental interest. The TRIGGER GENERATOR module receives these trigger signals and initiates a conversion, if the system is not busy with the previous event, and triggers the List Processor after a delay to read the event into its 128 KBytes buffer. TG also keeps track of the number of accepted triggers and when it reaches the user defined block-size it interrupts the computer. Reading of data by LP and the transfer of it to the computer are done in parallel by configuring the LP buffer in two 64 Kilobyte chunks. While it is collecting data into one buffer the other will get transferred to the computer memory by Direct Memory transfer. The singles mode data is converted by Canberra 8075 ADCs interfaced to home-made histogram generator modules located inside the CAMAC Crates. The 24Bit, 8K channel histograms are read by the computer whenever required. Another computer, TCP/IP networked to the server using Ethernet, provides the User Interface, Analysis and Display functions etc. There are several other computers networked to the server for transferring the data from the hard disk to cartridge tapes.

3.5.1.2 The Software

The Server:The server consists of two processes, called MAIN and STORE, running on the computer connected to the CAMAC highway. MAIN communicates to the client through two TCP/IP channels, one for commands from the client and other for sending data to the client for on-line analysis. In response to the INITIALIZE command the CAMAC system is configured and the START command enables the data collection and CAMAC interrupts. In response to the interrupts from CAMAC the MAIN process initiates a DMA transfer from one of the List Processor buffers to a Computer Shared Memory Buffer and configures the alternate LP buffer for further data collection. A user defined portion of data is sent to the client for on-line analysis and display. The MAIN process also receives and executes the commands like reading CAMAC histogram modules, pausing and resuming the acquisition, controlling the disk write etc. from the client. The STORE process reads the Shared Memory Buffer, does zero suppression, and save the data to a hard disk. The data is saved as a series of files each having the size of a cartridge tape. The disk is accessible by several computers through NFS and they store the data to tapes. The tapes write at a slower speed but the data rate is maintained by writing many files in parallel. The server is driven by interrupts and the data transfer from CAMAC is through DMA. This results in a very low usage of CPU time. It allows for more detailed processing of raw data in addition to the simple zero suppression it is doing at present. A screen-shot of the program GUI in the 2D spectrum mode is shown in figure 3.7

The Client: There are three processes running on the client side, the GRAPHICAL USER INTERFACE under X-windows, the ANALYSIS process and the RECEIVE process. These three processes along with two shared memory buffers, the RAW DATA BUFFER and SPECTRUM BUFFER, functions in the following manner. The user configures the desired spectra to be generated from various parameters by interacting with the GUI and this information is stored in the Spectrum Shared Memory. The GUI process also sends the user commands to the SERVER. The RECEIVE process accepts the raw data from the SERVER and stores it to the RAW DATA BUFFER buffer memory and wakes the Analyze process. The Analysis process processes the raw data according to the stored configuration and saves the output to the spectrum shared memory. The GUI displays the spectra on the screen. Time consuming On-line analysis is possible without affecting

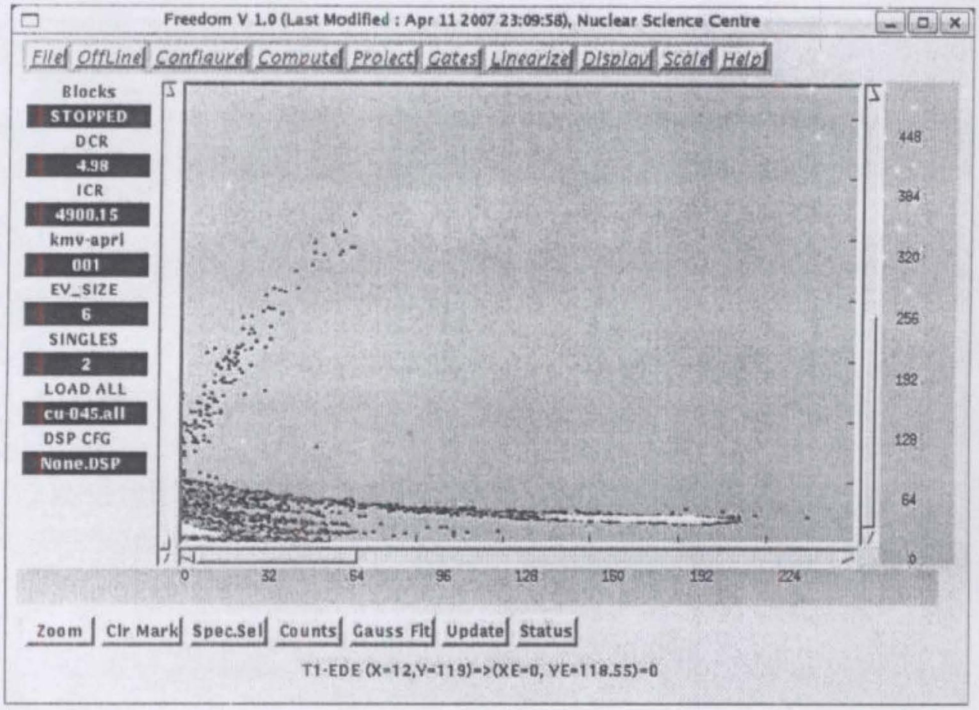

Freedom V 1.0 (Last Modified : Apr 11 2007 23:09:58), Nuclear Science Centre

Blocks
STOPPED
DCR
4.98
ICR
4900.15
kmv-aprl
001
EV_SIZE
6
SINGLES
2
LOAD ALL
cu-045.all
DSP CFG
None.DSP

T1-EDE (X=12,Y=119)->(XE=0, YE=118.55)=0

Figure 3.7: A screen-shot of the 'Freedom' Data Acquisition System.

the server performance. Any delay in processing may result in filling of the raw data buffer which makes the Receive process to accept and discards some data to allow the server to proceed at full speed. The GUI is implemented using the Athena Widgets. The user can interactively configure the CAMAC addresses of all the parameters associated with an event and a name, like Energy, Delta-E etc., is given to each of them for identification. One and Two dimensional Spectra can be defined by selecting any of these parameters. It is possible to do a wide range of logical and arithmetic operations on the raw data before displaying.

3.5.1.3 The results

Combining the inexpensive PC hardware with a powerful operating system has resulted in a very cost effective Data Acquisition and Analysis System. The typical event rates, of about 1 KHz with 30 parameters, generated by the current experiments has been handled easily. The system is able to handle a simulated trigger rate of about 7 KHz master trigger rate and an event size of 30 parameters, ie. acquiring and storing about 400 Kilobytes per second. The program can also run in an OFFLINE mode where data is read from the disk instead of on-line data.

From 1997 onwards, Freedom is being used for all the accelerator based experiments conducted at IUAC and later a high speed multi-crate version of it named CANDLE also has been developed to handle large systems like the Indian National Gamma Array (INGA). A low cost derivative of the same using the home-made CAMAC controllers also being used at IUAC and several other places including University of Calicut. Further development in this direction resulted in a radiation detection and analysis system that is affordable to Universities and colleges. The offline version of Freedom also gave the flexibility to the experimentalists from the universities to do the offline data analysis at their own place. It was developed using Free Software tools running on a GNU/Linux platform that could be freely distributed.

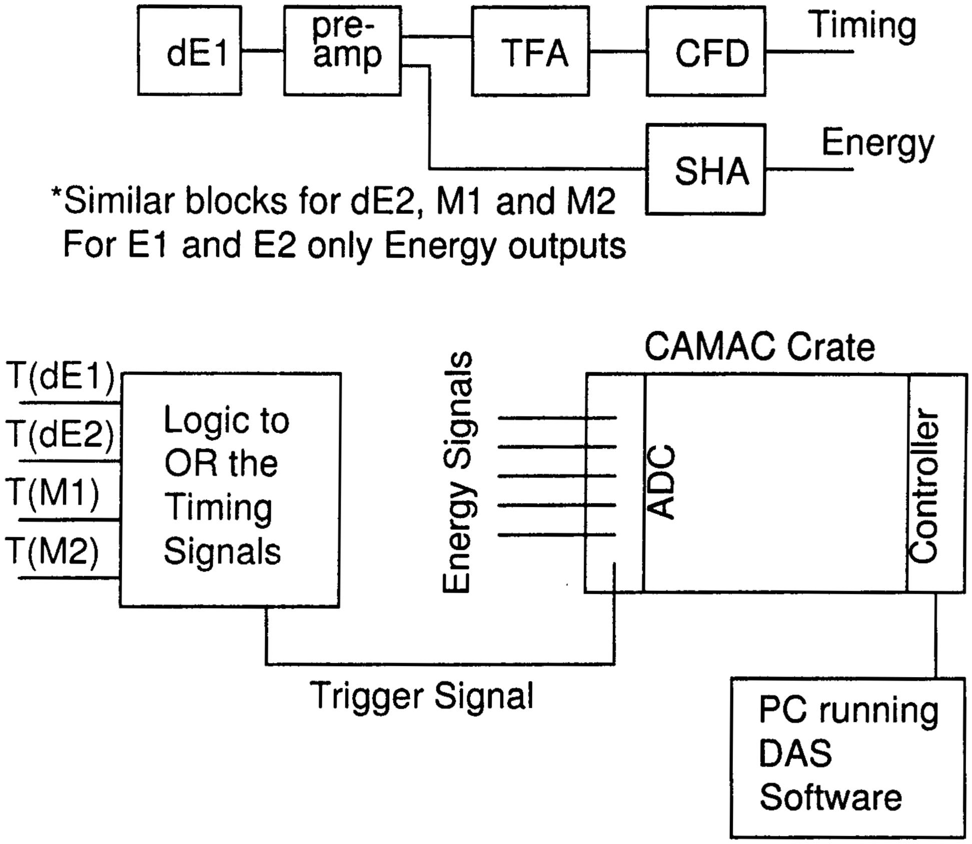

Figure 3.8: A block schematic of the Data Acquisition System hardware. The detector outputs are fed to the pre-amplifiers. The Shaping Amplifier, Timing Filter Amplifiers, Constant Fraction Discriminators and OR gates are implemented using NIM modules. The digitization of the energy signals are done by CAMAC ADC modules having multiple channels.

3.5.1.4 Data Acquisition Setup for Fission Experiment

Initial experiments we conducted, using the Pelletron at IUAC, used Freedom for data acquisition. Later experiments conducted, using the BARC-TIFR Pelletron, used LAMPS [Ambar] for data acquisition and analysis. LAMPS is again a list mode DAS running on Linux operating system and uses CAMAC hardware fore data collection. This system is being used at the BARC-TIFR Pelletron accelerator at Mumbai. For measuring the fission fragment angular distribution, the experimental setup is more or less similar whether Freedom or LAMPS is used for data acquisition. A schematic block diagram of the data acquisition setup used for collecting the fission data is shown in figure 3.8.

The experimental setup has two E-ΔE telescopes and two monitor detectors. All the energy signals are recorded whenever there is a signal from any of the ΔE detectors, which is considered as a valid event. The data acquisition system is triggered by the OR output of the timing outputs from these detectors. The monitor detector outputs should be recorded independent of the event mode signals. However, when the count rates are low the monitor detectors also can be included in the event, including their timing output also in the triggering logic. The energy outputs of the pre-amplifier are fed to the shaping amplifier. The output of the shaping amplifiers are connected to the pulse ADCs plugged into a CAMAC Crate. The CAMAC Crate is connected to the PC running the data acquisition software.

On the detection of a valid event all the ADCs are triggered and the output is stored to the computer. The E-ΔE signals are used for generating 2D plots and the monitor detector outputs are plotted as histograms to display the energy spectrum of scattered particles.

Bibliography

[Ajith 1997]	A Linux based Data Acquisition System at NSC, Ajith Kumar et. al, SANAI 97, BARC (1997)
[Ambar]	http://www.tifr.res.in/~pell/lamps.html
[Knoll 1978]	Glenn F. Knoll, Radiation Detection and Measurement, John Wiley & Sons Inc (1999)

Investigation of Fusion Reactions of Heavy Ions And Development of Necessary Instrumentation

A Thesis submitted to the University of Calicut
for the partial fulfillment of the requirements
for the degree of
Doctor of Philosophy in Physics

Ajith Kumar B.P.

Department of Physics
University of Calicut
May, 2007

Chapter 4

Study of ^{13}C + ^{232}Th Reaction

Angular distribution of fission fragments resulting from the decay of the compound nucleus formed by bombarding ^{232}Th target with different projectiles masses has been studied in the past. It has been reported that, at above barrier energies the anisotropy of angular distribution agreed with the Statistical Saddle Point Model (SSPM) predictions for small projectile masses. However, for heavier projectiles, the observed anisotropy exceeded the SSPM predictions for all energies. It is postulated [Ramamurthy 1990] that for mass asymmetry values less than the Bussinaro-Gallone [Businaro 1955] critical mass asymmetry, mass flow occurs from the projectile to the target and a fully equilibrated compound nucleus is formed. The decay of it results in an angular distribution as predicted by SSPM. For higher mass asymmetry values, the mass flow occurs from the target to the projectile and fission occurs through the formation of a di-nuclear system without ever forming a fully equilibrated compound nucleus. This results in larger observed anisotropies.

It has been reported that, at above barrier energies the results of ^{12}C+^{232}Th [Ramamurthy 1990, Mein 1997] followed the SSPM predictions but ^{14}N+^{232}Th [Behera 2001] showed deviations. The present study investigates ^{13}C+^{232}Th, whose mass asymmetry lies in between the above two systems, for an energy range spanning the barrier. If the above barrier results are in agreement with SSPM, it indicates that the ^{13}C+^{232}Th reaction proceeds through the formation of a fully equilibrated compound nucleus.

At near barrier energies both the systems exhibit anomalous anisotropy due to the ground state deformation of the target. Deformed targets with zero spin shows a sudden increase in anisotropy near the barrier and the results of ^{12}C+^{232}Th is reported by [Mein 1997]. Repeating the same using ^{13}C projectile will bring out the effect of non-zero projectile spin on the anomalous behavior near the barrier.

4.1 Experiment

To study the fusion-fission of ^{13}C+^{232}Th , we have bombarded a 1.8 mg/cm^2 thick thorium foil with ^{13}C beam. The fission fragments were recorded from 80^0 to 170^0 with respect to the direction of the beam, at 10^0 intervals using two E-ΔE telescopes, separated by 20^0, mounted on a rotatable table. A circular collimator having 5 mm diameter was placed in front of the fission detectors kept at distance of 12.7 cm from the target. Thin (~15 micron) Silicon Surface Barrier Detectors, SSBD, fabricated at BARC, are used as ΔE detectors. Bias voltages around 10 volts is applied to operate them in the fully depleted mode. Commercially available SSBDs having a thickness of 500 micron are used as the E detectors, biased to more than 100 volts. The detailed description of the experimental setup is given in the previous chapter.

We have used two monitor detectors in order to normalize the fission yield and also to calculate the absolute fission cross section. The first monitor detector was kept at 22^0 at a distance of 42.3 cm from the target, with a 1 mm diameter collimator. The second one was at 40^0 and 25.4 cm from the target and used a 2 mm collimator. The angle, distance and the opening of the detectors were selected to make the count rates comparable. The integrated beam current also was recorded using a current integrator.

The contribution from transfer induced fission for ^{12}C+^{232}Th in this energy region has been measured by Mein et al. [Mein 1997] and found to be less than 5% of the total cross section. In the case of ^{13}C projectile the neutron transfer channel can lead to the formation of ^{233}Th but fission following transfer is less probable since the formation of ^{233}Th at an excited state exceeding the fission barrier is not favorable from the Q value considerations. From the systematics [Kailas 1997] it is expected that fission following transfer will be less than 5% in this energy range. Since the expected contribution from transfer is not significant the folding angle measurements to separate the full momentum transfer fission events were not done.

The beam energy was varied from 60 MeV to 80 MeV, in the laboratory frame of reference, in 5 MeV steps and the fragment angular distribution is measured at each energy. For this purpose, the fission detector telescopes were first kept at, say 80^0 and 100^0. The ^{232}Th target was positioned at the center of the scattering chamber and ^{13}C beam of desired energy was allowed tobe incident at the centre of the target. Eventwise data were collected for sufficient time period required for obtaining reasonable statistical accuracy. One dimensional spectra were generated online for the monitor and the E and ΔE signals from both telescopes. Two dimensional spectra were also generated in order to separate the fission fragments from the elastically and inelastically scattered projectiles. From the 2D plots, total fission counts were extracted. The monitor counts were also noted from the monitor signal spectra. Typical plots were shown in figure 4.1.

In order to minimize the statistical error, around ten thousand fission events were accumulated at higher energies. At below barrier energies, it was restricted to thousand due to the very low cross section. The fission counts were taken from the 2D spectrum generated from the E-ΔE outputs. The ratio of the solid angles subtended by both the fission detectors were measured and correction is applied before comparing the counts from them. The measurements taken at different energies is shown in the tables 4.1.

4.2 Extraction of Anisotropy values

Data presented in table 4.1 is processed in the following manner. The fission detector yields from each angle are normalized using the monitor detector kept at 22^0. When the data is collected for the same angle from both the detectors, the normalized yields are added together. The statistical error in each detector output is given by $\frac{1}{\sqrt{N}}$, where N is the number of counts.

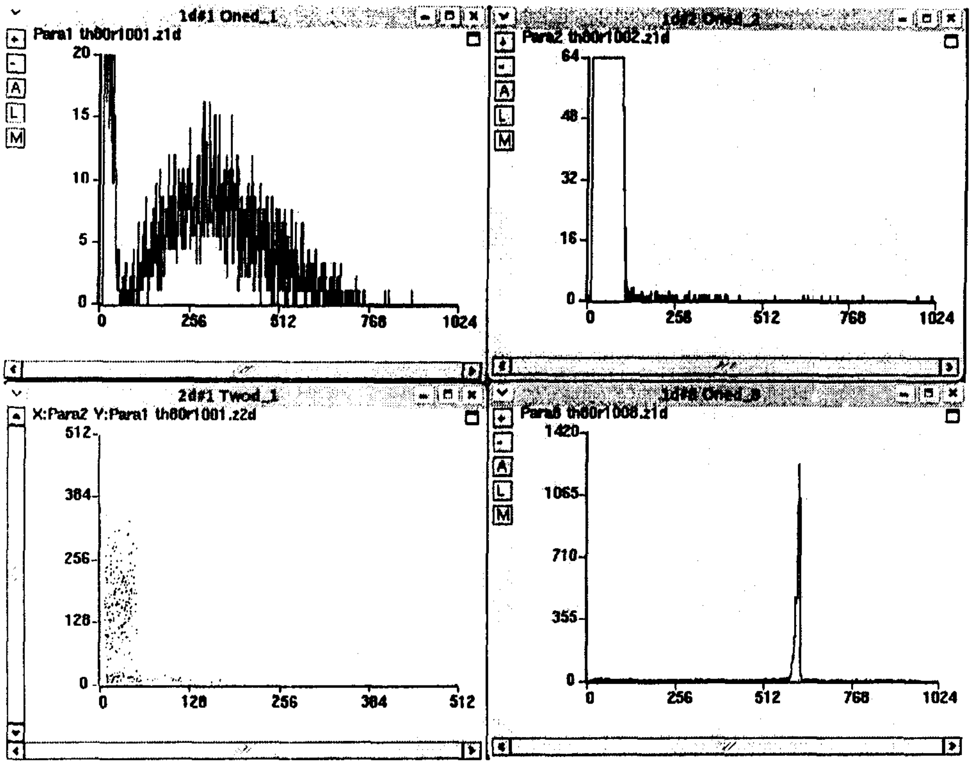

Figure 4.1: One and two dimensional spectra of the signals from the fission and monitor detectors. The top left one is the ΔE signal of a fission detector telescope showing the fission fragments. Fission counts are taken from the y-axis projection of the E-ΔE 2D spectra.

E_{lab}(MeV)	θ_{lab}	Fission	M_{22}	E_{lab}(MeV)	θ_{lab}	Fission	M_{22}
80	170	26768	28180	65	170	3050	79262
80	160	22326	24330	65	160	3023	79466
80	150	25016	28180	65	150	3100	79262
80	140	20475	24330	65	140	2995	79466
80	130	17665	22139	65	130	3081	83217
80	120	25360	34240	65	120	3082	84741
80	110	24525	32043	65	110	2990	86267
80	100	25790	34240	65	100	3255	91773
80	90	15270	19800	65	90	3109	86247
80	80	16700	20560	65	80	3423	91757
75	170	18780	34280	63	170	3000	199619
75	160	12140	22836	63	160	1766	123637
75	150	17920	34289	63	150	3000	199619
75	140	11270	22836	63	140	1763	123637
75	130	10120	20936	63	130	-	-
75	120	11600	24566	63	120	1968	138647
75	110	11093	23700	63	110	1897	157793
75	100	13068	29302	63	100	1810	151076
75	90	-	-	63	90	2001	157793
75	80	16600	34540	63	80	2020	151076
70	170	8376	36400	60	170	975	821335
70	160	5410	25105	60	160	390	323274
70	150	8105	36400	60	150	975	821335
70	140	5214	25105	60	140	390	323274
70	130	6678	32227	60	130	-	-
70	120	6613	33339	60	120	745	621660
70	110	6435	34541	60	110	-	-
70	100	7573	37035	60	100	655	595465
70	90	6976	34541	60	90	825	700934
70	80	7115	33200	60	80	730	595465

Table 4.1: The fission fragment angular distribution data for $^{13}C+^{232}Th$ reaction. Experiment done for projectile energies ranging from 60 to 80 MeV

Statistical error in fission counts is around 1% at higher energies and increases up to 3% due to the smaller number of events collected at low energies. While taking the sums and ratios of the detector counts, the standard error propagation formula

$$\sigma_u = \sqrt{\left(\frac{\partial u}{\partial x}\right)^2 \sigma_x^2 + \left(\frac{\partial u}{\partial y}\right)^2 \sigma_y^2 + ..} \tag{4.1}$$

is used for calculating the error in the derived quantity. Since the errors in the measurements of the detector solid angles and the angular position of the detectors are much smaller than the statistical error, they are not taken into account. The results are then transformed into the center of mass frame using Viola systematics [Viola 1985] ,which assumes symmetric mass division. The normalized fission yields are calculated as a function of angle at each energy value. Corrections are applied to the projectile energy before converting into the center of mass frame to account for the energy loss inside the thorium target. Energy of the projectile when it is half way through the target foil is used for the calculations.

In order to calculate the anisotropy, the results are fitted using the expression

$$W(\theta) = a + bP_2(\cos\theta) + cP_4(\cos\theta) \tag{4.2}$$

where P_2 and P_4 are Legendre polynomials.The anisotropy is defined as $A = W(180)/W(90)$, where W(180) and W(90) are the differential cross section at 180^0 and 90^0 respectively, and are obtained by the above fit. The measured differential fission cross section as a function of energy is shown in figure 4.2, where the solid curve is the obtained fit using equation 5.1. The anisotropies are calculated for each energy and the result is shown in figure 4.3. It can be seen that at above barrier energies the anisotropy decreases with energy and shows an upward trend near the barrier.

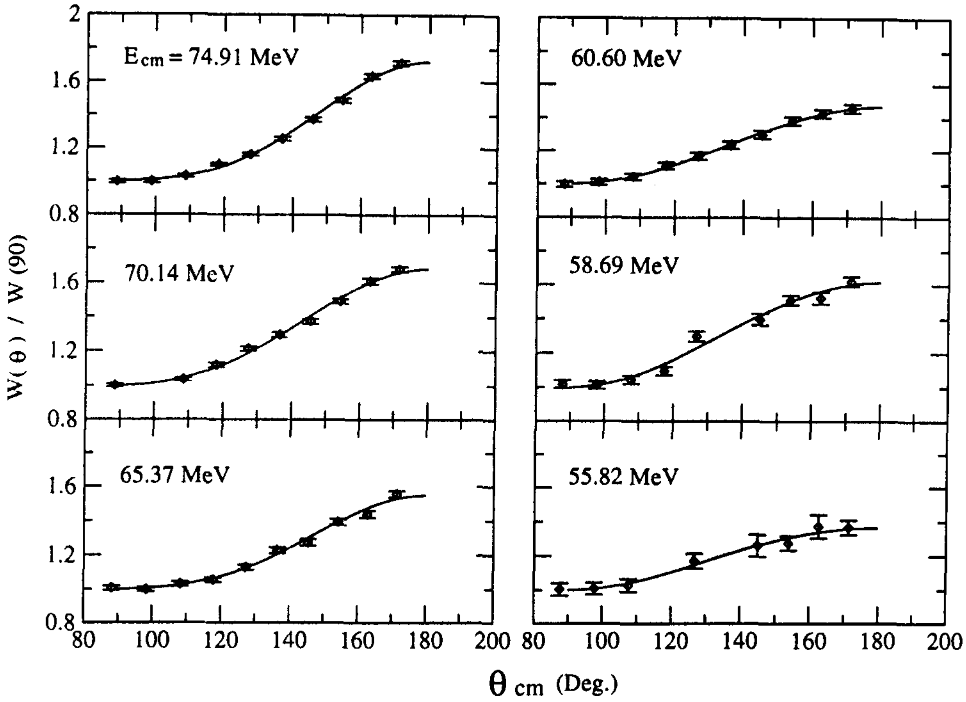

Figure 4.2: The measured fission fragment angular distributions of $^{13}C+^{232}Th$ system. The solid curve is obtained by fitting the experimental data using Legendre polynomials. All values are divided by W(90) to read the anisotropy value directly from the plot.

E_{cm}	$\sigma(E)$	σ_{err}
55.82	2.3	0.16
58.69	24.5	0.95
60.60	62.0	1.73
62.99	155.17	6.67
65.37	299.8	6.19
67.7	454.6	17.3
70.14	611.9	10.97
74.91	913.5	13.13

Table 4.2: Total fusion cross section data extracted from the fission yield data shown in table 4.1 except for energies 62.99 MeV and 67.7 MeV, that are from measurements done later.

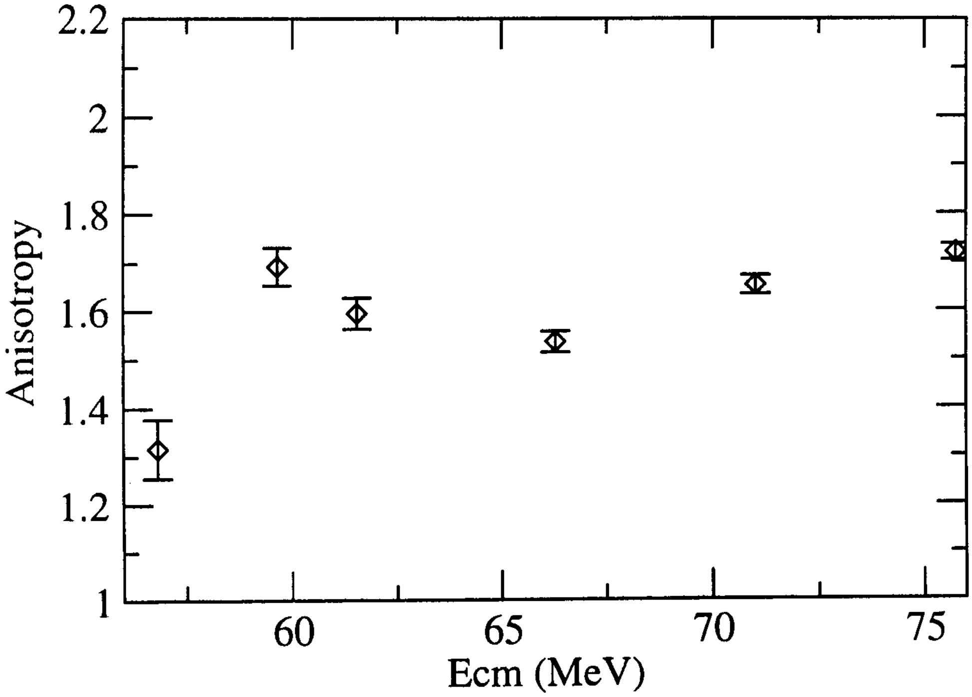

Figure 4.3: Anisotropy of fission fragment angular distribution for the $^{13}C + ^{232}Th$ system as a function of energy.

4.3 Extraction of Fission Cross-sections

The differential fission cross section is calculated using the equation

$$\frac{d\sigma_{fis}}{d\Omega}(\theta_{cm}) = \frac{1}{2}\frac{Y_{fis}}{Y_{mon}}\frac{d\sigma_R}{d\Omega}(\theta_{lab})\frac{\Omega_{mon}}{\Omega_{fis}}G \tag{4.3}$$

where G is the Jacobian of laboratory frame to center of mass frame transformation, Y_{fis} and Y_{mon} are the number of counts recorded by the fission and monitor detectors respectively, Ω_{fis} and Ω_{mon} are the solid angles and $\frac{d\sigma_R}{d\Omega}(\theta)$ is the Rutherford cross section. We make the assumption that all the events recorded by the monitor detector are due to Rutherford scattering.

The total fission cross-section $\sigma(E)$ can be obtained by integrating the differential cross section $\frac{d\sigma_{fis}}{d\Omega}(\theta)$ calculated in the previous section. This can be done by fitting the differential cross section data using the equation

$$\frac{d\sigma_{fis}}{d\Omega}(\theta) = a + b\cos^2\theta + c\cos^4\theta \tag{4.4}$$

and applying the extracted coefficients to the equation for total cross section

$$\sigma(E) = 4\pi\left(a + \frac{b}{3} + \frac{c}{5}\right) \tag{4.5}$$

The total fission cross sections calculated using the above formula are shown in table 4.2. Since the compound nucleus formed is highly fissile and the decay is almost totally by fission, the fusion cross section is assumed to be equal to the fission cross section. The fusion barrier distribution is obtained by differentiating $E\sigma(E)$ twice with respect to energy using the equation 4.6. The results are discussed in detail in the next sections along with the results of the theoretical calculations.

4.4 Data Analysis

The experimental data is analyzed in the following manner. The fusion cross section as a function of energy is calculated using the coupled channel code CCFUS. The barrier parameter is adjusted for the best agreement between

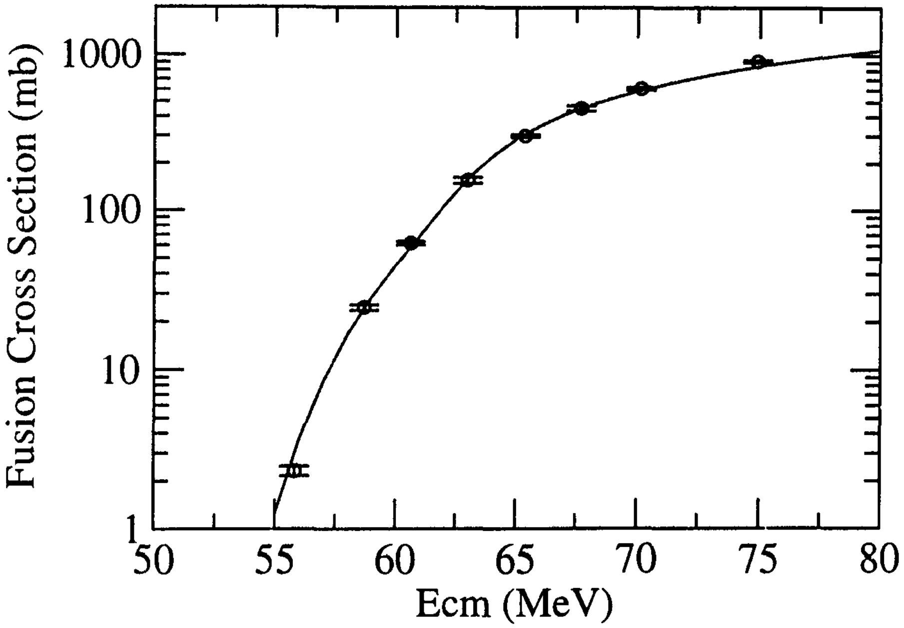

Figure 4.4: Fusion Excitation Function of the compound nucleus formed by ^{232}Th + ^{13}C reaction. The solid curve is the result of the coupled channel calculations done using the code CCFUS.

the calculated and measured cross sections. The corresponding value of $\langle \ell^2 \rangle$ is used in anisotropy calculations. The SSPM calculations are done using the equation 2.48 . The width of K distribution, temperature and the effective moment of inertia of the saddle point nucleus are calculated using the Sierk prescription [Sierk 1986] based on the Rotating Finite Range model, RFRM. The experimental anisotropy values are compared with SSPM results. Calculations are done using the Pre-Equilibrium Fission (PEF) model [Ramamurthy 1985, Thomas 2003] to explain the anomalous anisotropy at near barrier energies.

4.4.1 Theoretical calculation of Fusion cross sections

The fusion cross section values for ^{13}C + ^{232}Th are calculated using the simplified coupled channel code CCFUS [Dasso 1997]. The static deformation parameters $\beta_2 = 0.22$ and $\beta_4 = 0.09$ are used for ^{232}Th target with prolate

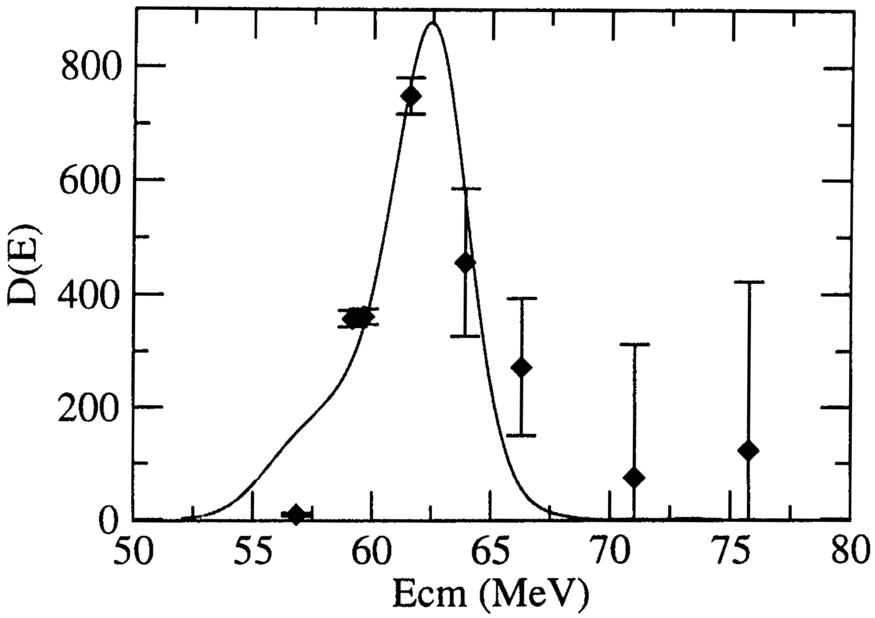

Figure 4.5: Fusion barrier distribution for the ^{232}Th + ^{13}C system. The solid curve is derived from the theoretical fusion cross section values calculated using CCFUS.

deformation. The code calculates the transmission coefficients for each partial wave using the Wong formula [Wong 1973] and integrate it to get the total cross section. The calculated values along with experimental results are shown in figure 4.4. It can be seen that the experimental data is well reproduced by the coupled channel code.

The fusion barrier distribution has been obtained from the cross section values using the equation

$$\frac{d^2(\sigma E)}{dE^2} = \left(\frac{(E\sigma)_3 - 2\,(E\sigma)_2 + (E\sigma)_1}{\Delta E^2}\right) \tag{4.6}$$

where value of 2 MeV is used for ΔE. The intermediate values are obtained by interpolating the data using a cubic spline interpolation. The result is shown in figure 4.5.

4.4.2 Anisotropy, SSPM calculations

The Saddle Point Statistical Model theory provides a simple relation between the anisotropy of fragment angular distribution A , angular momentum of the saddle point nucleus J and the projection K of it along the symmetry axis. The exact expression for angular distribution given by the equation 2.48 is used for doing the calculations. It can also be expressed by the approximate expression

$$A \approx 1 + \frac{\langle \ell^2 \rangle}{4K_0^2} \tag{4.7}$$

$$K_0^2 = T\frac{I_{eff}}{\hbar^2} \tag{4.8}$$

$$I_{eff} = \frac{1}{I_{\parallel}} - \frac{1}{I_{\perp}} \tag{4.9}$$

$$T = \sqrt{\frac{E_{cm} + Q - B_f(\ell) - E_{rot}(\ell) - E_n}{a}} \tag{4.10}$$

The parameters used in the above equations are briefly explained below along with some reference to the theoretical models used to compute them.

$\langle \ell^2 \rangle$ is the mean square angular momentum of the compound nucleus. We have calculated it using the coupled channel code CCFUS. The barrier parameter, input parameter used by the code to adjust the barrier properties, is chosen so that the calculated fusion cross section matches with the experimentally measured value. From equation 4.7 it can be seen that the anisotropy increases as a function of $\langle \ell^2 \rangle$. For very high angular momentum values, the potential energy pocket required to form the compound nucleus vanishes and the SSPM predictions becomes inapplicable.

K_0^2 represents the width of the K distribution, ie. the statistical spread in the value of K. Larger the value of K_0^2 , more isotropic is the fragment angular distribution. If fission has occurred before equilibrating in the K degree of freedom, a sharper K distribution will result due to the memory of entrance channel K distribution. Its value depends on the nuclear temperature and the effective moment of inertia calculations of which are explained below.

I_{eff} is the effective moment of inertia of the compound nucleus at the saddle point, which is function of deformation. The shape of the saddle point nucleus is related to the anisotropy through this parameter, larger the deviation from spherical shape, more the value of I_{eff}. Qualitatively it can be said that it is easier to tilt a shape that is closer to spherical shape and will result is a larger value of K_0^2. I_{eff} is calculated using the Sierk prescription [Sierk 1986] based on the Rotating Finite Range, RFRM. In this model the surface energy is calculated by assuming a Yukawa-plus-exponential nuclear potential incorporating the effect of the finite range of the nuclear force and the finite surface thickness of real nuclei. The Coulomb energy is calculated for a charge distribution with a realistic surface diffuseness.

T is the nuclear temperature decided by the energy available towards the excitation degrees of freedom of the compound nucleus. Only part of the total excitation energy, which is the sum of the kinetic energy in the center of mass frame and the Q value of the reaction, contributes to the temperature. The rotational energy and the RFRM fission barrier $B_f(J)$ is calculated using the Sierk prescription. The energy taken away by the evaporating neutrons E_n is calculated using the systematics suggested by Saxena et. al [Saxena 1994]. A value of 10 is used for the level density parameter a . Choosing a value of

E_{cm}	$\langle \ell^2 \rangle$	I_{eff}	B_{fis}	T	K_0^2	A
56.8	99	175.0	2.8	1.0	173.0	1.16
60.6	177	175.2	2.7	1.0	178.9	1.27
64.4	223	175.4	2.6	1.1	185.6	1.33
68.2	345	176.0	2.5	1.1	193.3	1.49
72.0	492	177.1	2.3	1.1	201.6	1.67
75.8	646	178.7	2.2	1.2	210.2	1.84

Table 4.3: The values of Anisotropy as a function of Energy calculated using SSPM, for ^{13}C + ^{232}Th reaction in an energy range spanning the Coulomb barrier. The intermediate parameters are also tabulated.

9 made no change at the lower end, 55 MeV, but the calculated value of A increased by 2% at 76 MeV.

The anisotropy values calculated using SSPM are shown in table 4.3. It can be seen that both $\langle \ell^2 \rangle$ and K_0^2 increase with energy and anisotropy increases slightly because the former increases more rapidly. The effective moment of inertia does not depend on energy very much. Within the energy range of consideration, the temperature is below the fission barrier. At below barrier energies the SSPM results are not in agreement with the experimental results. The deviations are attributed to the ground state deformation of the target and theoretical calculations are done using the Pre-Equilibrium Fission model as described in the next section.

4.4.3 Pre-Equilibrium Fission Model Calculations

According to PEF model, systems having mass asymmetry, $\alpha = (A_T - A_P)/(A_T + A_P)$, larger than the Bussinaro-Gallone [Businaro 1955] critical mass asymmetry α_{BG} proceed towards compound nucleus formation before undergoing fission. For $\alpha < \alpha_{BG}$, the composite system relaxes towards a symmetric di-nuclear system leading to non-compound nucleus fission. For deformed targets, it is possible to form a composite system with contact configuration more elongated than the unconditional saddle point configuration by interacting with the tip of the target. In this case the system relaxes towards a symmetric di-nuclear system without forming a compound nucleus. PEF assumes a shifting of the Businaro-Gallone point towards higher mass

E_{cm}	A	E_{cm}	A	E_{cm}	A
54	1.45	62	1.52	70	1.60
56	1.47	64	1.47	72	1.68
58	1.51	66	1.46	74	1.77
60	1.55	68	1.52	76	1.85

Table 4.4: Anisotropy values calculated using the PEF model for ^{232}Th + ^{13}C system.

asymmetries due to the channel coupling effects. According to PEF, the fragment angular distribution is an admixture of the CNF and PEF components and is given by the equation [Thomas 2003]

$$W(\theta) = \sum_{\beta} P_{\beta}[W_{CNF}(\beta,\theta) + W_{PEF}(\beta,\theta)] \qquad (4.11)$$

where P_{β} is the probability of fusion from the eigen channel β. W_{CNF} and W_{PEF} are the fragment angular distributions for CNF and PEF modes of fission. The Anisotropy values calculated using PEF model is shown in table 4.4.

4.4.4 Discussion of Results

We have measured the fusion cross sections and fission fragment angular distribution at energies spanning the coulomb barrier, around 64 MeV in the center of mass frame, for the ^{12}C + ^{232}Th system. The fusion cross sections are compared with coupled channel calculations. The anisotropy values above barrier is compared to SSPM calculations and with the results obtained for the same target using nearby projectile masses. Anisotropies near the barrier are compared with SSPM and PEF model predictions.

4.4.4.1 Fission Cross Sections

Since the compound nucleus formed from the reaction ^{13}C+^{232}Th is highly fissile and the decay is almost totally by fission, the fusion cross section is assumed to be equal to the fission cross sections. The fusion cross sections are calculated using the coupled channel code CCFUS. The calculated cross

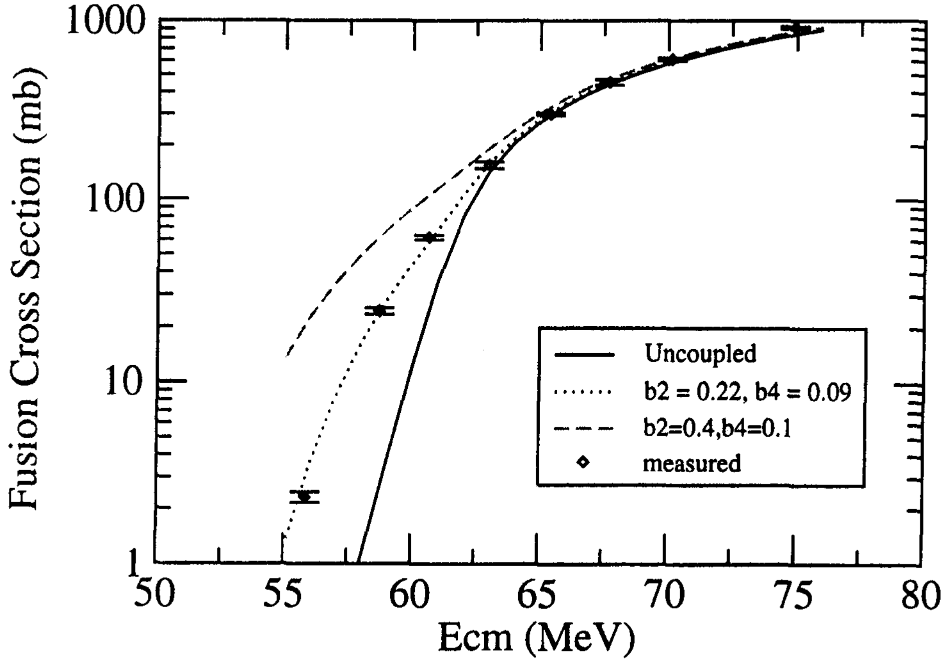

Figure 4.6: Fusion cross sections for the ^{13}C+^{232}Th system. Experimental values are shown along with results of coupled channel calculations using different values for the deformation parameters β_2 and β_4.

sections along with the measured values are shown in the figure 4.6. It can be seen that at above barrier energies ($\approx 64MeV$), the fusion cross sections can be calculated from the transmission probability through a one dimensional radial potential. At below barrier energies the results obtained without considering the channel coupling effects are lower than the measured values. Including the channel coupling effects due to the static deformation of the target gave results tallying with the measurements. The deformation parameters $\beta_2 = 0.22$ and $\beta_4 = 0.09$ gave best agreement with experimental results.

The extracted barrier distribution is shown in figure 4.5. The gradual increase of the barrier on the low energy side is expected from the ^{232}Th target having prolate deformation. However, the experimental points taken at 5 MeV energy interval is not enough to clearly show this effect. The value

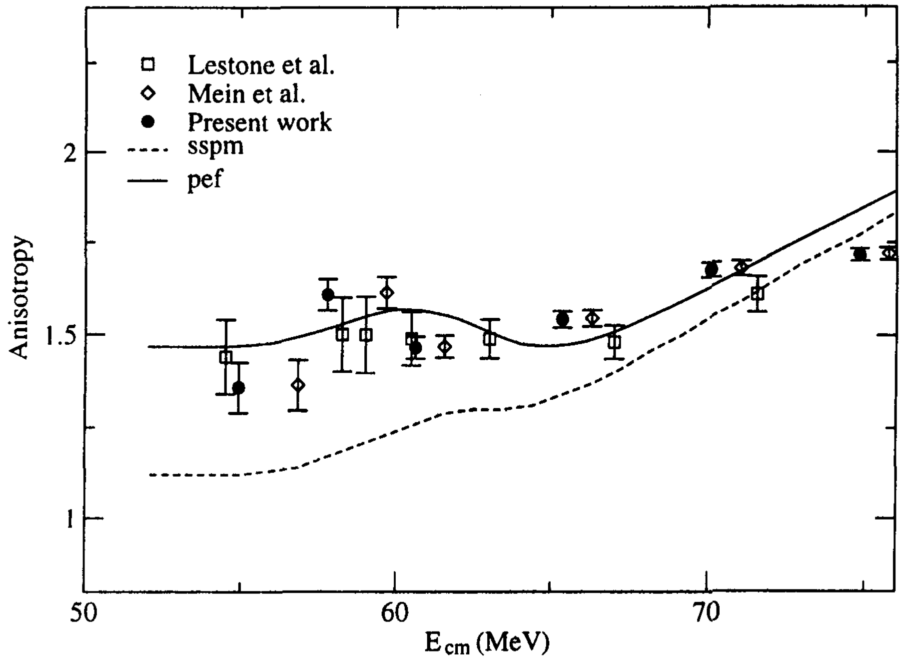

Figure 4.7: Measured fission fragment anisotropies along with the calculated values from SSPM and PEF models. Data from Lestone and Mein are for ^{12}C + ^{232}Th system. The present work shows ^{13}C + ^{232}Th.

of calculated$\langle \ell \rangle$ is found to be from around $7\hbar$ to $25\hbar$ in the explored energy range.

4.4.4.2 Anisotropies above the Coulomb Barrier

The anisotropies extracted from the fits to the angular distributions are plotted in figure 4.7. The data of ^{12}C + ^{232}Th system measured by Lestone et al. [Lestone 1997] and Mein et al. [Mein 1997] are also shown for comparison. The dotted line is the prediction of SSPM. It can be seen that though the anisotropies are in agreement with the SSPM values at above barrier energies , this is much different from the behavior of the ^{14}N+^{232}Th system reported by Behera et al. [Behera 2001] which shows strong deviation from SSPM at above barrier energies also. Anisotropies for ^{14}N projectile energies, where the effect of channel couplings is small, the dynamics of the

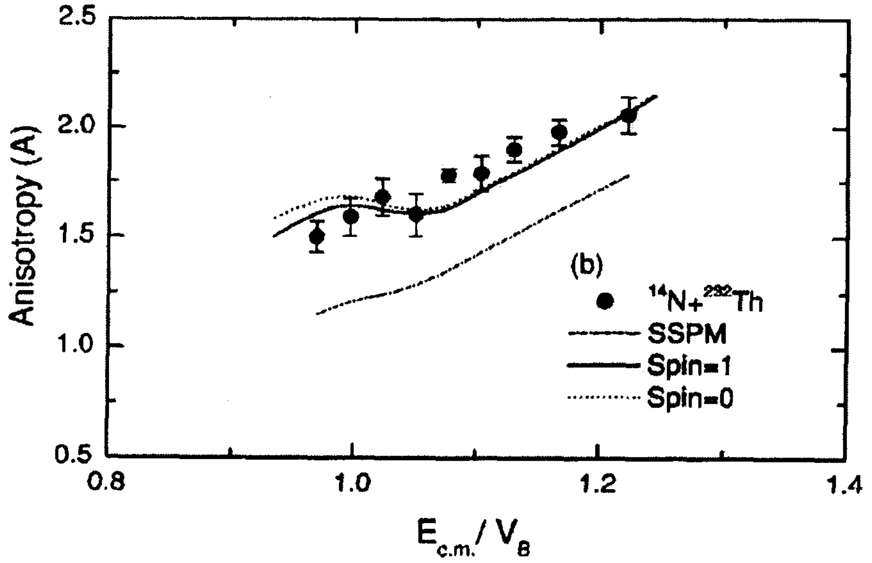

Figure 4.8: Values of anisotropy for ^{14}N+^{232}Th reported by Behera et. al.

^{13}C+^{232}Th system is much similar to the ^{12}C+^{232}Th system which evolves into a mono-nuclear configuration after contact unlike the ^{14}N+^{232}Th system which proceeds to a di-nuclear complex after contact. The latter gives rise to the presence of PEF events thereby increasing the anisotropies. It is found that at above barrier energies the anisotropy values for ^{12}C and ^{13}C are consistent with SSPM predictions within error limits while the values for ^{14}N are significantly higher. The results imply that the transition from CNF to an admixture of CNF and PEF takes place between ^{13}C and ^{14}N for ^{232}Th target.

4.4.4.3 Anisotropies at Below Barrier Energies

From figure 4.7 it can be seen that the measured anisotropy reduces gradually with energy at above barrier energies. Just below the barrier the anisotropy shows an upward trend and comes down again with further reduction of energy. The behavior is similar to the available data for ^{12}C + ^{232}Th [Lestone 1997, Mein 1997]. The effect of projectile spin on anisotropy was studied by Nayak et. al [Nayak 2000] for ^{10}B (spin = 3^+) and ^{11}B (spin

– 3/2$^-$) and they have reported significant deviation from SSPM for ^{11}B + ^{232}Th . However for ^{13}C (spin = 1/2) and ^{12}C (spin = 0) the difference in projectile spin does not make any observable change in anisotropy. The PEF model calculation [Thomas 2003] results for ^{13}C + ^{232}Th are also shown in figure 4.7.

Bibliography

[Behera 2001]	Behera B R et al, Phy. Rev. C64 (2001)
[Behera 2004]	Behera B R et al, Phy. Rev. C69 (2004)
[Businaro 1955]	Businaro U L et al, IL Nuovo Cimento, Vol. I.N.4 (1955)
[Dasso 1997]	Dasso C H et al, Comp. Phy. Comm. 46(1987)
[Lestone 1997]	Lestone J P et al., Phy. Rev. Vol. C56(1997)
[Mein 1997]	Mein J C et al, Phy. Rev. C55(1997)
[Nayak 2000]	Nayak B K et al, Phy. Rev. Vol. C62(2000)
[Kailas 1997]	Kailas S, Phys. Rep. 284, 381 (1997) and references theirin.
[Ramamurthy 1990]	Ramamurthy V S et al, Phy. Rev. Lett. 65,25(1990)
[Saxena 1994]	Saxena A et al, Phy. Rev. C Vol. 49(1994)
[Sierk 1986]	Sierk A J, Phy. Rev. C Vol. 33(1986)
[Thomas 2003]	Thomas R G et al, Phy. Rev. C67 (2003)
[Viola 1985]	Viola V E et al, Phy Rev C31 (1985)

Investigation of Fusion Reactions of Heavy Ions And Development of Necessary Instrumentation

A Thesis submitted to the University of Calicut
for the partial fulfillment of the requirements
for the degree of
Doctor of Philosophy in Physics

Ajith Kumar B.P.

Department of Physics
University of Calicut
May, 2007

Chapter 5

Study of ^{13}C + ^{235}U Reaction

The ^{235}U nucleus has prolate deformation and a spin of 7/2 in its ground state. Bombarding ^{235}U with ^{13}C projectile results in the formation of the ^{248}Cf compound nuclues, which decays mainly through fission. We have measured the fission fragment angular distribution and the fission cross section for the ^{13}C + ^{235}U system from 63 MeV to 84 MeV beam energies. The measured anisotropies are compared with PEF model calculations and the total fission cross sections with coupled channel calculations.

Comparing the results of ^{13}C + ^{235}U with ^{13}C + ^{232}Th, zero spin target, reveals the effect of target spin. The results are also compared with ^{12}C + ^{235}U to look for any change in anisotropy due to the difference in projectile spins. The ^{13}C + ^{235}U reaction proceeds through the ^{248}Cf compound nucleus, that has been studied earlier using ^{237}Np + ^{11}B, ^{236}U + ^{12}C and ^{232}Th + ^{16}O reactions to study the effect of mass asymmetries [Kailas 1999]. The present study will further investigate this aspect.

5.1 The Experiment

To study the fusion-fission of ^{13}C+^{235}U , we have bombarded a 200 μg/cm^2 thick ^{235}U deposited on Aluminium backing. The experimental setup used is similar to the one used for studying the ^{13}C+^{232}Th reaction. The fission fragments were recorded from 80^0 to 170^0 with respect to the direction of the

E_{lab}(MeV)	θ_{lab}	Fission	M_{40}	E_{lab}(MeV)	θ_{lab}	Fission	M_{40}
84	170	1978	1680	80	170	2170	2459
84	160	2019	1769	80	160	2041	2414
84	150	1954	1680	80	150	1997	2464
84	150	1784	1621	80	150	1928	2459
84	140	2276	2146	80	140	1990	2599
84	140	1987	1789	80	140	1837	2414
84	130	2070	2176	80	130	1872	2414
84	130	1697	1621	80	130	1810	2464
84	120	2037	1959	80	120	1851	2599
84	120	1989	2146	80	120	1687	2457
84	110	1989	2176	80	110	1771	2414
84	110	1966	2189	80	110	1675	2485
84	100	3207	3985	80	100	1695	2457
84	100	1876	1959	80	100	1609	2544
84	90	1971	2189	80	90	1635	2485
84	80	3415	3985	80	80	1694	2544
75	170	727	1611	70	170	616	3939
75	160	720	1626	70	160	637	3741
75	150	726	1611	70	150	724	4041
75	150	672	1626	70	150	609	3939
75	140	687	1620	70	140	740	4177
75	140	650	1626	70	140	614	3741
75	130	669	1639	70	130	771	4650
75	130	639	1626	70	130	700	4041
75	120	634	1665	70	120	672	4177
75	120	672	1620	70	120	657	4368
75	110	645	1639	70	110	733	4650
75	110	630	1553	70	110	700	4769
75	100	638	1632	70	100	-	-
75	100	628	1665	70	100	-	-
75	90	616	1553	70	90	721	4769
75	80	628	1632	70	80	675	4431

Table 5.1: The fission fragment angular distribution data for ^{13}C+^{235}U reaction. Experiment done for projectile energies ranging from 70 MeV and 84 MeV

E_{lab}(MeV)	θ_{lab}	Fission	M_{40}	E_{lab}(MeV)	θ_{lab}	Fission	M_{40}
65	170	379	20331	63	170	91	21354
65	160	400	20903	63	150	125	20841
65	150	397	20331	63	140	146	23944
65	150	315	17133	63	120	99	17835
65	140	409	20903	63	110	133	23345
65	140	292	16144	63	110	107	20356
65	130	320	17133	63	100	148	22895
65	130	263	15001	63	100	95	18148
65	120	319	15676	63	90	130	23345
65	120	296	16144	63	80	135	22895
65	110	297	15001				
65	110	286	15114				
65	100	345	19284				
65	100	290	15676				
65	80	363	19284				

Table 5.2: The fission fragment angular distribution data for ^{13}C+^{235}U reaction. Experiment done for projectile energies ranging for 63 MeV and 65 MeV

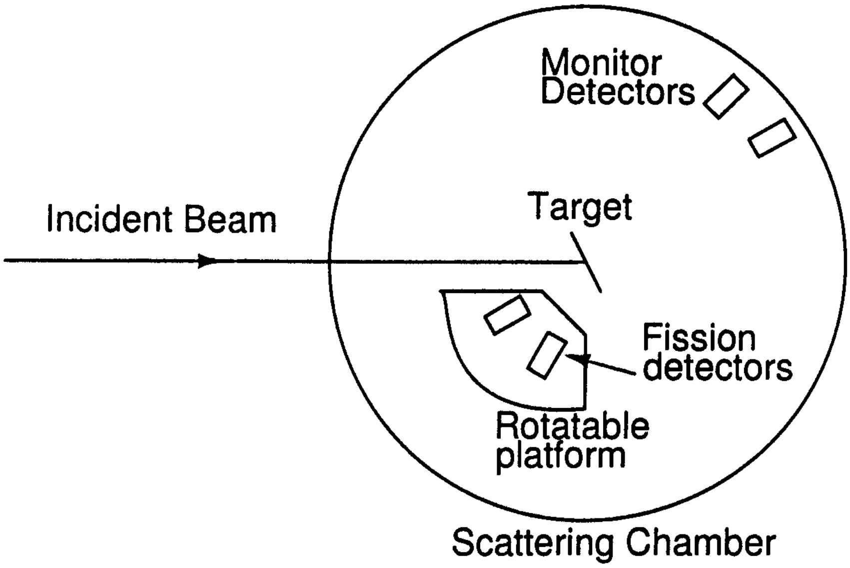

Figure 5.1: Experimental setup to the fission fragment angular distribution of $^{235}U + ^{13}C$ system. The fission detectors are mounted on a rotatable to cover from $80^0$to 170^0. The monitor detectors are kept at $40^0$and 50^0angles.

beam, at 10^0 intervals using two E-ΔE telescopes, separated by 20^0, mounted on a rotatable table as shown in figure 5.1. A circular collimator having 4 mm diameter was placed in front of the fission detectors kept at distance of 14.12 cm from the target. Two thin (12 and 14 microns) Silicon Surface Barrier Detectors were used as ΔE detectors. Bias voltages around 5 Volts were applied to operate them in the fully depleted mode. SSBDs having a thickness of 300 micron are used as the E detectors, biased to more than 100 volts.

We have used two monitor detectors, one kept at 40^0 at a distance of 39.52 cm from the target and the other at 50^0 and 36.98 cm from the target. Both detectors used a 2 mm collimator. The angle, distance and the opening of the detectors were selected to make the count rates comparable. The 40^0 detector is user for normalizing the fission yield and also to calculate the absolute fission cross section. The second one was kept just for cross checking purpose.

The beam energy was varied from 60 MeV to 84 MeV, in the laboratory frame of reference, in 5 MeV steps and the fragment angular distribution is measured at each energy. The barrier energy is around 68.7 MeV in the laboratory frame. Two to three thousand fission events were accumulated at higher energies but it was restricted to around five hundred at near barrier energies due to the very low cross section. The fission counts were taken from the 2D spectrum generated from the E-ΔE outputs. The ratio of the solid angles subtended by both the fission detectors were measured and correction is applied before comparing the counts from them. The measurements taken at different energies is shown in the tables 5.1 and 5.2.

The contribution from transfer induced fission for ^{12}C+^{235}U in this energy region has been measured by Lestone et al. [Lestone 1997] and found to be less than 5% of the total cross section. In the case of ^{13}C projectile the neutron transfer channel can lead to the formation of ^{236}U but the Q value is much less than the fission barrier. Since the expected contribution from transfer is not significant the folding angle measurements to separate the full momentum transfer fission events were not done.

5.2 Analysis of Data

The anisotropies and fusion cross sections are extracted from the experimental data. The effect of entrance channel mass asymmetry and target spin are investigated by comparing with results from the literature. Fission cross sections are compared with the fusion cross sections calculated using the coupled channel code CCFUS. Theoretical calculation of anisotropy is done using PEF model.

5.2.1 Extraction of anisotropies and fission cross sections

Data presented in tables 5.1 and 5.2 are processed in the same manner as explained in the previous chapter. The fission detector yields are normalized using the monitor detector for each angles. When the data is collected for

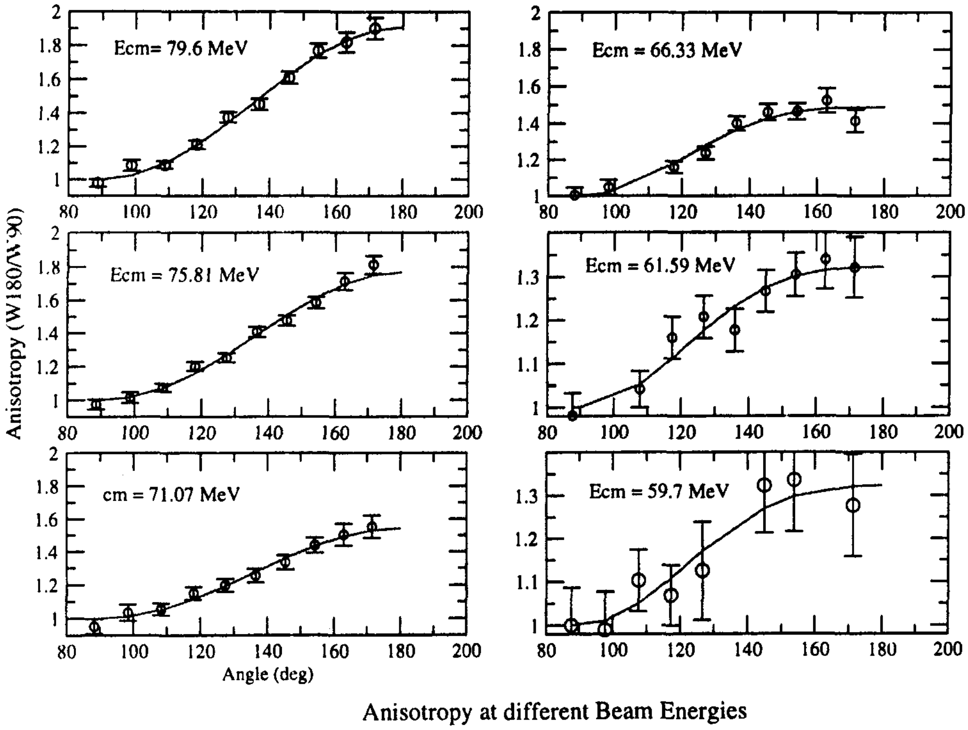

Figure 5.2: Measured fission fragment angular distribution for ^{13}C+^{235}U. The solid curve is the fit done using Legendre polynomials.

E_{cm}(MeV)	$A = W(180)/W(90)$	A_{err}	$\sigma(E)$mb	σ_{err}	
79.60	1.90	0.05	968	37	
75.81	1.77	0.05	790	30	
71.07	1.54	0.06	494	28	
66.33	1.49	0.06	221	12	
61.59	1.32	0.08	30	2.2	
59.70	1.32	0.15	10	1.5	

Table 5.3: Total measured anisotropies and total fission cross sections of ^{13}C + ^{235}U system at different energies.

the same angle from both the detectors, the normalized yields are added together. In order to calculate the anisotropy, results are fitted using the expression

$$W(\theta) = a + bP_2(\cos\theta) + cP_4(\cos\theta) \tag{5.1}$$

where P_2 and P_4 are Legendre polynomials. The fission yields along with the curve fit using equation 5.1 are shown in figure 5.2.

The absolute values of differential fission cross sections are calculated using the equation

$$\frac{d\sigma_{fis}}{d\Omega}(\theta_{cm}) = \frac{1}{2}\frac{Y_{fis}}{Y_{mon}}\frac{d\sigma_R}{d\Omega}(\theta_{lab})\frac{\Omega_{mon}}{\Omega_{fis}}G \tag{5.2}$$

where G is the Jacobian of laboratory frame to center of mass frame transformation, Y_{fis} and Y_{mon} are the number of counts recorded by the fission and monitor detectors respectively, Ω_{fis} and Ω_{mon} are the solid angles and $\frac{d\sigma_R}{d\Omega}(\theta)$ is the theoretical value of Rutherford cross section. Here we assume that all the counts from the monitor detector are due to Rutherford scattering.

The total fission cross-section $\sigma(E)$ can be obtained by integrating the differential cross section $\frac{d\sigma_{fis}}{d\Omega}(\theta)$. This is done by fitting the differential cross section data using the equation

$$\frac{d\sigma_{fis}}{d\Omega}(\theta) = a + b\cos^2\theta + c\cos^4\theta \tag{5.3}$$

and applying the extracted coefficients to the equation for total cross section

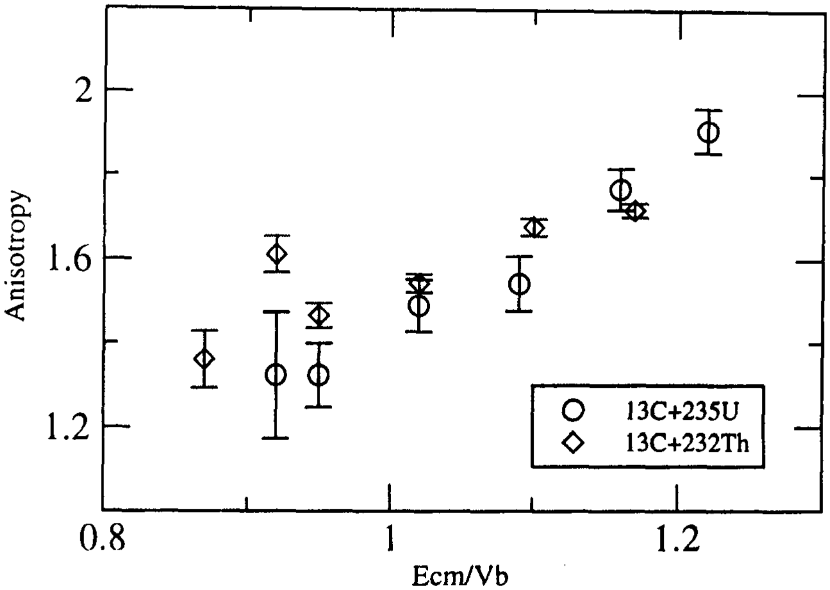

Figure 5.3: The anisotropies resulting from ^{13}C projectile on ^{232}Th (zero spin) and ^{235}U (spin −7/2) targets.

$$\sigma(E) = 4\pi\left(a + \frac{b}{3} + \frac{c}{5}\right) \tag{5.4}$$

Since the compound nucleus formed is highly fissile and the decay is almost totally by fission, the fusion cross section is assumed to be equal to the fission cross section. The extracted anisotropies and total fission cross section values are shown in table 5.3.

5.2.2 Effect of Target and projectile Spins

Deformed targets exhibit anomalous anisotropies at near barrier energies. For zero spin targets, the anisotropy plot shows a bump near the barrier, as evident from the ^{13}C + ^{232}Th data shown in figure 5.3. For targets having large ground state spins this effect is somewhat washed out and the anisotropy shows a monotonous variation with energy. The physical origin of this can be qualitatively explained using the following arguments. For a target having prolate deformation, the amount of Coulomb repulsion the projectile has to

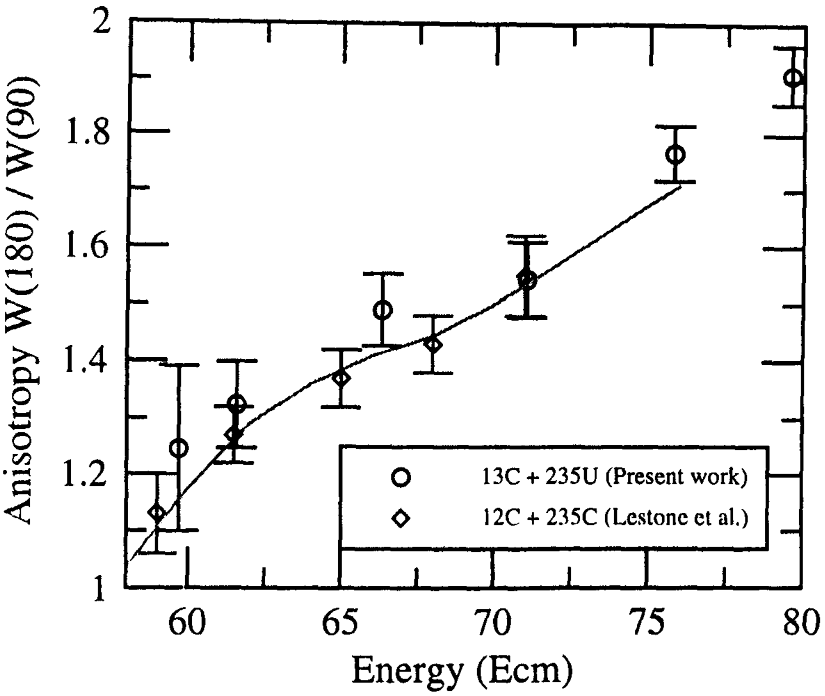

Figure 5.4: The anisotropies resulting from ^{12}C (spin zero) and ^{13}C (spin 1/2) projectiles on ^{235}U (spin 7/2) target.

overcome is less when the interaction is with the tip of the target and at near and below barrier energies this type of interaction becomes dominant. When the interaction is mostly with the tips, the rotation will be perpendicular to the nuclear symmetry axis and the K distribution will be strongly peaked around $K = 0$, if the target spin is zero. For a target spin of I the K distribution will be peaked at $\pm I$ and will be distributed among all the possible values of M, projection of J along the beam axis, which results in a reduction of anisotropy at the barrier according to the equation 2.47. Figure 5.3 shows a comparison of ^{13}C projectile on ^{232}Th and ^{235}U targets results. It can be seen that the anisotropy shows an increase just below the barrier for the zero spin ^{232}Th target while the ^{235}U (spin = 7/2) shows a smooth variation.

Similar effect has also been reported earlier by Lestone et. al. [Lestone 1997]

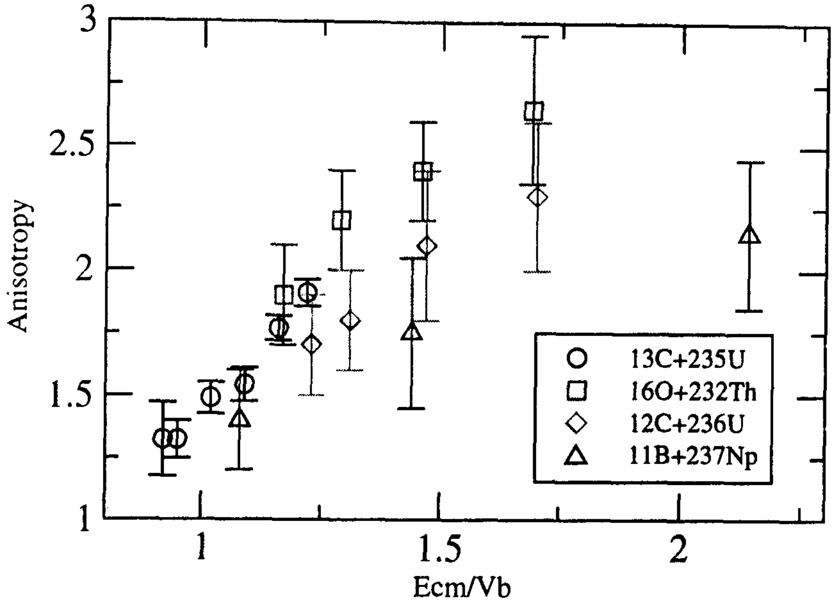

Figure 5.5: Measured anisotropies ^{248}Cf compound nucleus formed by different entrance channels. The ^{13}C + ^{235}U data is from the present study and the rest are from[Kailas 1999].

for ^{12}C + ^{235}U system. Lestone has explained this based on the Entrance Channel Dependant K State Model by Vorkapic et. al. [Vorkapic 1995]. Figure 5.4 compares the results ^{12}C and ^{13}C projectiles on the ^{235}U target, which shows that the difference in the projectile spin is not sufficient to make any noticeable change in the behavior of anisotropy. The PEF model calculation results for ^{13}C + ^{235}U is also shown. It can be seen that the PEF model explains the results well [Thomas 2003].

5.2.3 Effect Entrance Channel Mass Asymmetry

The ^{13}C + ^{235}U reaction proceeds through the ^{248}Cf compound nucleus. The same compound nucleus has been studied earlier using the entrance channels ^{11}B + ^{238}U ,^{12}C + ^{236}U and^{16}O + ^{232}Th [Kailas 1999] having different mass asymmetries. Any dependency on the entrance channel will result in different values of anisotropy from the same compound nucleus. It has been reported

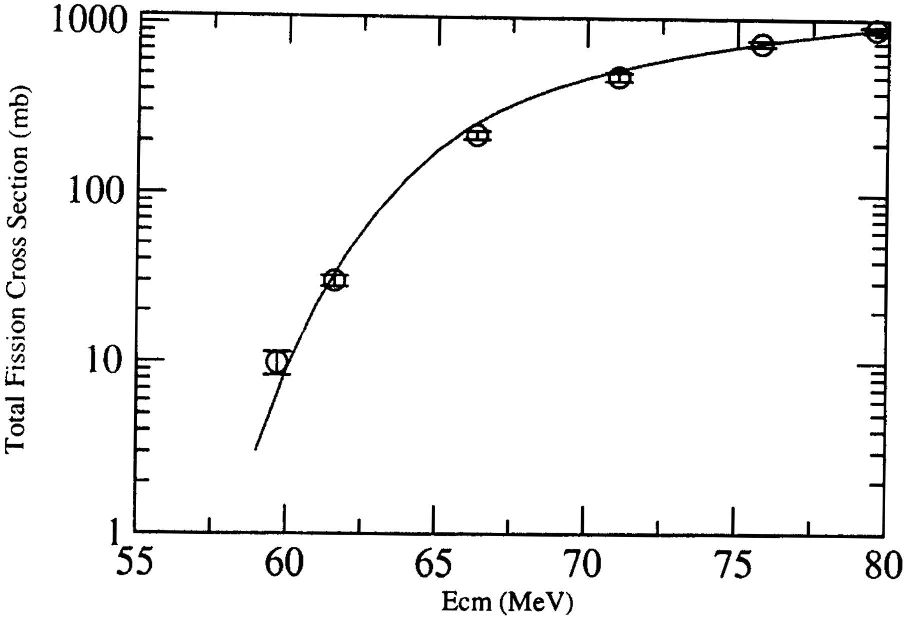

Figure 5.6: Measured fusion cross sections for ^{13}C + ^{235}U at different energies. The solid curve shows the values calculated using the coupled channel code CCFUS.

that the dependency on the entrance channel mass asymmetry vanishes at energies more than 30% above the barrier. Below that the anisotropies depend on the mass asymmetry. The present data along with the results from the literature are shown in figure 5.5. It can be seen that the anisotropy of ^{13}C + ^{235}U falls in between the ^{12}C + ^{236}U and^{16}O + ^{232}Th systems. We do not have data at higher energies where the entrance channel effects vanishes.

5.2.4 Comparing fusion cross sections with coupled channel calculations

The fusion cross section values for ^{13}C + ^{235}U are calculated using the simplified coupled channel code CCFUS [Dasso 1997]. The static deformation parameter $\beta_2 = 0.20$ is used for ^{235}U nucleus. . The calculated values along with experimental results are shown in figure 5.6. The average angular momentum $\langle \ell \rangle$varies from around 6 to 25 when the projectile energy is changed from 56 to 80 MeV.

Bibliography

[Behera 2001] Behera B R et al, Phy. Rev. C64 (2001)

[Behera 2004] Behera B R et al, Phy. Rev. C69 (2004)

[Businaro 1955] Businaro U L et al, IL Nuovo Cimento, Vol. I.N.4 (1955)

[Dasso 1997] Dasso C H et al, Comp. Phy. Comm. 46(1987)

[Lestone 1997] Lestone J P et al., Phy. Rev. Vol. C56(1997)

[Mein 1997] Mein J C et al, Phy. Rev. C55(1997)

[Nayak 2000] Nayak B K et al, Phy. Rev. Vol. C62(2000)

[Kailas 1999] Kailas S et al, Phy Rev C Vol 59(1999)

[Kailas 1997] Kailas S, Phys. Rep. 284, 381 (1997) and references theirin.

[Ramamurthy 1990] Ramamurthy V S et al, Phy. Rev. Lett. 65,25(1990)

[Saxena 1994] Saxena A et al, Phy. Rev. C Vol. 49(1994)

[Sierk 1986] Sierk A J, Phy. Rev. C Vol. 33(1986)

[Thomas 2003] Thomas R G et al, Phy. Rev. C67 (2003)

[Viola 1985] Viola V E et al, Phy Rev C31 (1985)

[Vorkapic 1995] Vorkapic D et al. Phy Rev C Vol 52(1995)

Investigation of Fusion Reactions of Heavy Ions And Development of Necessary Instrumentation

A Thesis submitted to the University of Calicut
for the partial fulfillment of the requirements
for the degree of
Doctor of Philosophy in Physics

Ajith Kumar B.P.

Department of Physics
University of Calicut
May, 2007

Chapter 6

Discussion and Conclusion

6.1 Present work

In this study we have measured the fission fragment angular distribution and fission cross sections of ^{13}C + ^{232}Th and ^{13}C+^{235}U systems [Ajith 2005, Ajith 2006]. The former was studied in order to investigate the effect of entrance channel mass asymmetry and projectile spin on the fission fragment anisotropy and the latter to study the effect of target spin. Anisotropies and fission cross sections were measured for both the systems at energies spanning the Coulomb barrier. The results are compared with SSPM and PEF model theories. Total fission cross sections are measured for both the systems. Since the compound nuclei formed is highly fissile, the fusion and fission cross sections are almost the same. The cross section results are compared with the predictions of the coupled channel code CCFUS. The fusion barrier distributions were also extracted.

6.1.1 The ^{13}C + ^{232}Th system

Earlier studies using the same target showed that the anisotropies followed SSPM predictions for ^{11}B and ^{12}C projectiles [Kailas 1999] but showed deviation for ^{14}N projectile [Behera 2004]. It was suggested that the NCN fission mechanisms starts contributing when the mass asymmetry is below the Bussinaro-Gallone critical mass asymmetry (α_{BG}) [Ramamurthy 1985].

The present system, having a mass asymmetry between the ^{12}C and the ^{14}N projectiles, is found to follow the SSPM predictions. This implies that for ^{13}C, the fission proceeds through compound nucleus formation. The results are very similar to that of ^{12}C, which suggests that the spin and mass of the extra neutron is not having any measurable impact on the fission mechanism.

Deformed targets exhibit anomalous anisotropy at near and below barrier energies. This has been observed in the present study also. This effect is attributed to the preferential interaction with the tips of the target at below barrier energies, ie. the energy is not sufficient to overcome the Coulomb barrier when approached from the sides. The PEF model explains this effect by the shifting of (α_{BG}) due to channel coupling effects. The experimental data shows agreement with the PEF predictions.

6.1.2 ^{13}C+^{235}U

The ^{13}C+^{235}U system was studied to investigate the effect of target spin at near barrier energies. This was earlier reported for ^{13}C+^{235}U system [Lestone 1997]. A large value of target spin washes out the bump in the anisotropy curve near the barrier, which can be explained by the following arguments. When the interaction is mostly with the tips, the rotation will be perpendicular to the nuclear symmetry axis and the K distribution will be strongly peaked around $K = 0$, if the target spin is zero. For a target spin of I the K distribution will be peaked at $\pm I$ and will be distributed among all the possible values of M, projection of J along the beam axis, which results in a reduction of anisotropy at the barrier according to the equation. The results of ^{232}Th (zero spin) and ^{235}U (spin = 7/2) was compared and the later shows a monotonous change in the anisotropy with energy. The results are in agreement with the PEF calculations.

Results of ^{13}C+^{235}U are also compared with that of ^{12}C on the same target. The non-zero spin of the projectile is not making any measurable difference in the anisotropy. The compound nucleus formed in this reaction is ^{248}Cf, that has been studied earlier for different entrance channels like ^{11}B + ^{238}U ,^{12}C + ^{236}U and^{16}O + ^{232}Th [Kailas 1999]. Present results are not drastically different.

6.2 Future Plans

Results of the present studies are in agreement with SSPM predictions for above barrier energies. This implies that the reaction proceeds through compound nucleus formation. However, at higher energies the fusion barrier becomes comparable to the temperature where the validity of SSPM may be doubtful. Further increase in energy will result is the vanishing of the potential pocket required to form the compound nucleus. Measuring the anisotropy at these energies and comparing with SSPM will provide some information about the fusion barrier and the critical angular momentum.

Fusion cross sections are very low below the barrier and understanding the channel coupling effect require good statistics. For this purpose an array of telescopes to measure the differential cross sections simultaneously is desirable. Work on a making such an array using gas ΔE detectors and solid state E detectors has been started and will continue it. Other aspects like reduction of noise by placing vacuum compatible pre-amplifiers inside the detector mount also may be explored.

Bibliography

[Ajith 2005] Ajith Kumar et al, Phy Rev C Vol 72(2005)

[Ajith 2006] Ajith Kumar et al, Proc. of the DAE/BRNS Symp. on Nucl. phy. (2006)

[Behera 2004] Behera B R et al, Phy. Rev. C69 (2004)

[Kailas 1999] Kailas S et al, Phy Rev C Vol 59(1999)

[Lestone 1997] Lestone J P et al., Phy. Rev. Vol. C56(1997)

[Ramamurthy 1990] Ramamurthy V S et al, Phy. Rev. Lett. 65,25(1990)